Universidade de São Paulo
Instituto de Física

O Grupo de Renormalização da Matriz Densidade Aplicado a Sistemas Quânticos Abertos

Heitor Peres Casagrande

Orientador: Prof. Dr. Gabriel Teixeira Landi

Dissertação de mestrado apresentada ao Instituto de Física da Universidade de São Paulo, como requisito parcial para a obtenção do título de Mestre em Ciências.

Banca Examinadora:
Prof. Dr. Gabriel Teixeira Landi - IFUSP
Profa. Dra. Maria Carolina de Oliveira Aguiar - UFMG
Profa. Dra. Krissia de Zawadzki - Northeastern University

São Paulo
2019

FICHA CATALOGRÁFICA
Preparada pelo Serviço de Biblioteca e Informação
do Instituto de Física da Universidade de São Paulo

Casagrande, Heitor Peres

O grupo de renormalização da matriz densidade aplicado a sistemas quânticos abertos. São Paulo, 2019.

Dissertação (Mestrado) – Universidade de São Paulo. Instituto de Física. Depto. de Física dos Materiais e Mecânica

Orientador: Prof. Dr. Gabriel Teixeira Landi
Área de Concentração: Física da Matéria Condensada /Termodinâmica Quântica

Unitermos: 1. Fenômenos de transporte; 2. O grupo de renormalização da matriz de densidade; 3. Sistemas quânticos abertos; 4. Cadeias de spin; 5. Métodos computacionais.

USP/IF/SBI-082/2019

University of São Paulo
Physics Institute

The Density Matrix Renormalization Group Applied to Open Quantum Systems

Heitor Peres Casagrande

Supervisor: Prof. Dr. Gabriel Teixeira Landi

Dissertation submitted to the Physics Institute of the University of São Paulo in partial fulfillment of the requirements for the degree of Master of Science.

Examining Committee:
Prof. Dr. Gabriel Teixeira Landi - IFUSP
Prof. Dr. Maria Carolina de Oliveira Aguiar - UFMG
Prof. Dr. Krissia de Zawadzki - Northeastern University

São Paulo
2019

To my family

Acknowledgments

”Nature seems to exist for the excellent. The world is upheld by the veracity of good men: they make the earth wholesome. They who lived with them found life glad and nutritious. Life is sweet and tolerable only in our belief in such society; and actually or ideally we manage to live with superiors. We call our children and our lands by their names. Their names are wrought into the verbs of language, their works and effigies are in our houses, and every circumstance of the day recalls an anecdote of them.” - Ralph Waldo Emerson (1803-1882).

It has always been, at least for myself, extremely remarkable how some have the singular ability of summing up grand, transcendental feelings in the flick of a pen, for I haven’t been able to find a more virtuous quote that fits so perfectly to my ever blessed experience not with science alone, but with the ones who make it, and with the ones that partake in such a divine enterprise.

I’d certainly start with my father, Douglas, which was able to balance the somewhat oppressive nature of an authority with the divine encouragement and understanding that only a life-long teacher is able to conceive. The same is true for my mother, Beatriz, which would surely and unwinking go to the limit of all that is possible to further advance my journey a single inch. They had, have and will forever more have all of my gratitude, love and utmost respect. I have yet to be bestowed a more magnificent gift. Muito obrigado.

Not only in the bosom of my family I have been blessed. For each step I took pointed me towards a competent and passionate ensemble of colleagues, friends and professors, with whom I’ve learnt much more than I’d think it would be possible. Such is the spectacle of being alive. Notably, the colleagues with which I had the pleasure of a more extended acquaintanceship as we have been travelling similar paths; particularly, Rafael Magaldi, Leonardo Barbosa, Geovane Grossi, William Malouf, Otavio Molitor, Jader Pereira, Artur Lacerda, Franklin Rodrigues, Bruno Ortega, as well as the much welcome and needed

other friends I made along the way.

I also extend my gratitude to my supervisor, Professor Gabriel Landi, and it can't be overstated how fruitful and pleasant the last two years have been. His faith in each particular talent is palpable and heartfully honest, and by each day I had a new incentive to push forward, as there's not one moment in which I haven't received his sincere attention and enthusiasm. It's been a privilege and a pleasure. Take the aforementioned quote to heart.

I thank the brazilian funding agency CNPq for the financial support provided for this work.

” If you can fill the unforgiving minute
With sixty seconds’ worth of distance run,
Yours is the Earth and everything that’s in it,
And-which is more- you’ll be a Man, my son!”
-Rudyard Kipling, If

Abstract

Open quantum systems have been studied for a long time, and albeit there's extensive literature detailing its various aspects, the complexity of the dynamics dictated by the environment and by quantum correlations within the system make it so that much is still unknown. The complexity introduced by quantum correlations instill highly non-trivial features, so that computational simulations are a viable route in studying such systems, which present, as it has been known for a long time, a myriad of rich, interesting phenomena. In this dissertation we implement an open-system version of the density matrix renormalization group, called oDMRG, suited for applications of thermal transport in one-dimensional spin chains. We have successfully implemented a routine to treat a wide range of systems. From the analytical results available for the XXZ model, a bench-mark was made and our results are found to be in agreement with those of previous works, and the simulations are viable in a common desktop computer. This dissertation puts forth the basic tools of oDRMG and may be of use for a variety of future studies in quantum transport and quantum thermodynamics.

Keywords: Transport Phenomena, The Density Matrix Renormalization Group, Open Quantum Systems, Spin Chains, Computational Methods

Resumo

A física que rege a dinâmica de sistemas quânticos abertos tem sido estudada há bastante tempo e, dessa forma, existe uma extensa gama de trabalhos sobre suas propriedades. No entanto, a complexidade de tais sistemas é aumentada devido a suas características inerentemente quânticas, bem como a interação com o ambiente, de forma que ainda há muito a se descobrir. Essa complexidade torna propício o uso de ferramentas numéricas para o estudo de tais sistemas. Nesta dissertação nós implementamos um versão do algorítimo do grupo de renormalização da matriz densidade para sistemas abertos, a que chamamos oDMRG, adequada para aplicações de transporte em cadeias uni-dimensionais. Tal rotina consegue tratar um variada gama de sistemas. Usando os valores analíticos disponíveis para o modelo XXZ, nós testamos o código, e nossos resultados concordam com os de trabalhos anteriores. Adicionalmente, as simulações podem ser realizadas num computador comum, não sendo necessário elevado poder de processamento. Essa dissertação estabelece, portanto, as ferramentas básicas do oDMRG e pode vir a ser usada para uma grande variedade de estudos futuros em transporte e termodinâmica quântica.

Palavras-chave: Fenômenos de Transporte; O Grupo de Renormalização da Matriz Densidade; Sistemas Quânticos Abertos; Cadeias de Spin; Métodos Computacionais.

Contents

List of Figures

Chapter 1

Introduction

Usually, when studying the behaviour of quantum systems, one might look at an atom, a harmonic oscillator, or even an electron trapped between two potential barriers. In reality, this setup is not always factual, since the system might not be, as most of the time is not, entirely isolated from everything else, being instead in contact with a certain portion of an environment. For a more realistic approach, one should therefore consider open quantum systems [1].

Coupling the system to an environment most likely guarantees that the problem being dealt with will become more complicated. For the particular case of quantum systems coupled to thermal baths, these complications would arise from non-locality, entanglement between each subsystem, and the sorts of quantum effects that would create non-trivial interactions between the particles. As there's no classic analog to these kinds of correlations [2], the study of these problems is novel and has many interesting new properties, namely in transport phenomena [3] and relaxation towards equilibrium [4], which may attain for possible novel technologies[5] [6]. These can be perceived as many-body effects, leading the study to the branch of quantum many-body problems.

As this implies, the problem at hand would be, then, a highly complex task in which a number of interactions play a role in the dynamics, and although a small portion of these problems may be actually treated analytically, usually via techniques such as Bethe-ansatz or Yang Baxter [7] [8], trying to tackle most of them in this manner will eventually lead to impossible tasks.

That's why the state-of-the-art approach to these kinds of problems have steered towards numerical simulations in the last years, and this trend is reinforced as the interest in these systems steadily grow, given the prospect of possible technologies to be developed,

such as the recent proposition of quantum computation using cold trapped ions [5], or the conception of a rectification-based diode [6] in the quantum framework.

As so, a wide array of simulation methods have surfaced, and have since then been polished and excellently studied by many groups [9] [10] [11] [12]. Initially, approximations related to mean-field approaches, being the most trivial and less computationally demanding, thrived. But a breakthrough followed, as the renormalization groups proved themselves to be more elegant while not prohibitive to simulate and work with [13] [14].

These methods were, then, boosted by recent advancements in Tensor Networks usage, whose powerful information storage structures made possible to hasten simulations even more. Particularly in the study of quantum systems, tensor networks pose a keen *ansatz* and subsequent approximations. This is due to the notion that, even though quantum systems description might take up exponential amounts of memory, which would in turn augment the associated Hilbert Space, the physics of such problems might not occur in the entirety of such space, but would instead take place in minor portions of it, which is dictated by an area law [15]. By, therefore, shrewdly diminishing the Hilbert Space, a simulation of its dynamics and important physical aspects might then, be possible, whilst posing a good approximation for the actual thing. This new prospect has since shed new light in the computational study of quantum systems, and important advancements and results have become frequent.

One particular work has extended the available methods of the density matrix renormalization group to open quantum systems, while making acute use of tensor networks representation techniques when describing the quantum state, in the form of a Matrix Product State [12]. This new approach for such problems, proved to be extremely promising, in both the realm of simulation techniques, as well as the physics related to these systems. Our work has been, in this sense, to develop an implementation of such a technique that is both reliable and easy to use, and also procedurally intelligent, aiming at lowering the computational and memory costs when simulating open systems, while progressively sharpening the physical properties guesses that might be of interest.

This work aims to implement such method by means of the open-source tensor library *ITensor* [16], and by doing so, it aspires to help groups that lack the state-of-the-art numerical tools to approach complicated problems relating to open quantum systems physics.

1.0.1 Dissertation overview

This dissertation verses over the previous works made on the subject of general simulations of quantum systems, and then presents new results in the XXZ chain transport coupled to two baths kept at different temperatures. In the following chapter, we revisit the foundations of Open Quantum Systems with some examples and also look at how to apply the concepts developed in the literature to our particular set of problems.

In chapter 3, we get into specifics of spin chains and the physics relating the coupling to thermal baths. Some interesting results in the literature, as well as the questions yet to be approached, are presented.

Chapters 4 and 5 both treat the simulation methods, namely with tensor networks in chapter 4, and their applications on the density matrix renormalization group approach, in chapter 5. Chapter 4 contains the foundations of Tensor Networks, and simple calculations done by the algorithms that were used in this work. Finally, chapter 5 contains a brief overview of the DMRG history and its applications, as well as some more technical results.

The remaining results are presented in chapter 6, where we present results for the energy convergence to the non-equilibrium steady-state, flux spin convergence, magnetization and transport regimes, making full use of the developed algorithm to look the physics of the XXZ-chain systems coupled to thermal baths.

Chapter 2

Open quantum systems

2.1 Lindblad master equations

In the case of closed systems, the system is isolated from every other possible interaction, and as so, the time evolution is described by the action of unitary operators on the system. However, for the case of open quantum systems, this isn't optimal, as in such scenarios, due to the fact that there's some kind of environment associated, the system eventually experiences dissipation, that is, it exchanges energy with the surroundings. Therefore it is not possible to study these systems by unitary operators alone [1].

Instead, when looking at open systems, one might prefer looking at a master equation, which states how the density matrix associated to that system changes over time, and by coupling the environment on to the system. The dynamical equation of Lindblad is the usual approach, with it being a broader look at the von Neumann equation,

$$\frac{d\rho}{dt} = -i[H, \rho], \tag{2.1}$$

which would describe the behaviour of the density matrix ρ of a closed system governed by a Hamiltonian. Indeed, the case is a bit more complex, as our system is in contact with baths. These baths are modeled following the dissipative effects of the environment, and the equation 2.1 we had before receives a new term, and becomes

$$\frac{d\rho}{dt} = -i[H, \rho] + D(\rho), \tag{2.2}$$

where $D(\rho)$ is called the Lindblad dissipator. The study of these dynamics mainly focuses

on the *steady-state* of the system, in this case a *non-equilibrium steady state* (NESS) due to the presence of the environment. Its behavior in such case is illustrated in the example that follows.

2.1.1 Dephasing noise

This is, indeed, the simplest example of a master equation acting on a qubit, whose Hamiltonian can be expressed as

$$H = \frac{\Omega}{2}\sigma_z. \tag{2.3}$$

Where the constant Ω relates to the energy gap in the system, and σ_z is the pauli-z matrix. By looking at the master equation as in 2.20, with

$$D(\rho) = \frac{\gamma}{2}(\sigma_z\rho\sigma_z - \rho), \tag{2.4}$$

we reach

$$\frac{d\rho}{dt} = -i[H,\rho] + \frac{\gamma}{2}(\sigma_z\rho\sigma_z - \rho), \tag{2.5}$$

Where the second term attains for the action of the environment. There's different ways to characterize such interactions, another one which will be approached in the next session. In this particular case, the dissipator term γ is the coupling constant to the environment, and as γ goes to zero, then the unitary dynamics are recovered.

Let us assume a general density matrix ρ parametrized as

$$\rho = \begin{pmatrix} p & q \\ q* & 1-p \end{pmatrix}, \tag{2.6}$$

and by plugging it back in Eq.2.5, we can derive time-independent functions for each variable p and q. Doing the algebra we get a simple set of equations:

$$\boxed{\begin{aligned} &\frac{dp}{dt} = 0 && \rightarrow && p = p_0 \\ &\frac{dq}{dt} = -(i\Omega + \gamma) && \rightarrow && q(t) = q_0 e^{-(i\Omega+\gamma)t} \end{aligned}} \tag{2.7}$$

Therefore $|q|$ shall decrease exponentially, dissipating the coherence of the system in the measure of how strong the coupling with the environment is, which is what one would expect, while the diagonal elements of the density matrix won't change. After enough time, the system will relax to a state without any coherence, which is just a statistical mixture, meaning that the system loses its quantum features. This is portrayed in Fig.2.1.

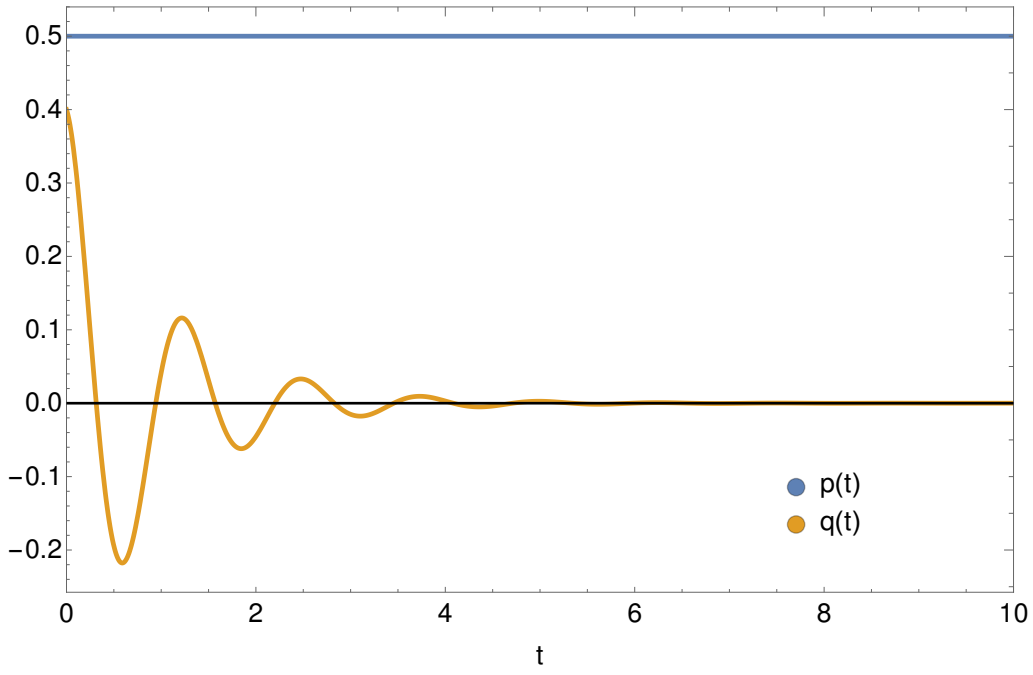

Figure 2.1: Evolution of the populations $p(t)$ and coherence $q(t)$ in the Dephasing noise example. One can see the exponential decrease in $q(t)$ while $p(t)$ remains constant. Parameters used: $q_0 = 0.4, \Omega = 5, \gamma = 1, p_0 = 0.5, f = 0.5$

This is an interesting look at how the environment is able to affect a certain system, as in this case the quantum probabilities will then be changed into classical.

2.1.2 Amplitude damping at finite temperature

For a more complex case, let's now look at the amplitude damping at finite temperature example, which is described by the master equation:

$$\frac{d\rho}{dt} = -i[H,\rho] + \gamma(1-f)\Big[\sigma_-\rho\sigma_+ - \frac{1}{2}\{\sigma_+\sigma_-,\rho\}\Big] + \gamma f\Big[\sigma_+\rho\sigma_- - \frac{1}{2}\{\sigma_-\sigma_+,\rho\}\Big], \quad (2.8)$$

where the σ_+ and σ_- are Pauli raising/lowering operators, and the factor γ is the coupling strength between dissipator and qubit. Additionally, the value f plays the role of the temperature in which the bath is. This kind of bath is the one we shall use in the study of open XXZ chain. If we take the Hamiltonian to be, as in the previous example,

$$H = \frac{\Omega}{2}\sigma_z, \tag{2.9}$$

and if we define

$$D[L] = L\rho L^\dagger - \frac{1}{2}\{L^\dagger L, \rho\}, \tag{2.10}$$

then Eq. 2.8 can be cast into the form

$$\frac{d\rho}{dt} = -i\frac{\Omega}{2}[\sigma_z, \rho] + \gamma(1-f)D[\sigma_-] + \gamma f D[\sigma_+]. \tag{2.11}$$

Aditionally, one can again represent a general density matrix ρ as:

$$\rho = \begin{pmatrix} p & q \\ q_* & 1-p \end{pmatrix}, \tag{2.12}$$

which can be combined with Eq.2.11, and will lead to a pair of equations,

$$\boxed{\begin{array}{lll} \dfrac{dp}{dt} = \gamma(f-p) & \rightarrow & p(t) = p_0 e^{-\gamma t} + f(1-e^{-\gamma t}) \\ \\ \dfrac{dq}{dt} = -(i\Omega + \frac{\gamma q}{2}) & \rightarrow & q(t) = q_0 e^{-(i\Omega+\gamma/2)t} \end{array}} \tag{2.13}$$

In this case, besides decoherence, there's also alteration in the populations, noted by the alteration in $p(t)$. This can be seem in Fig.2.2.

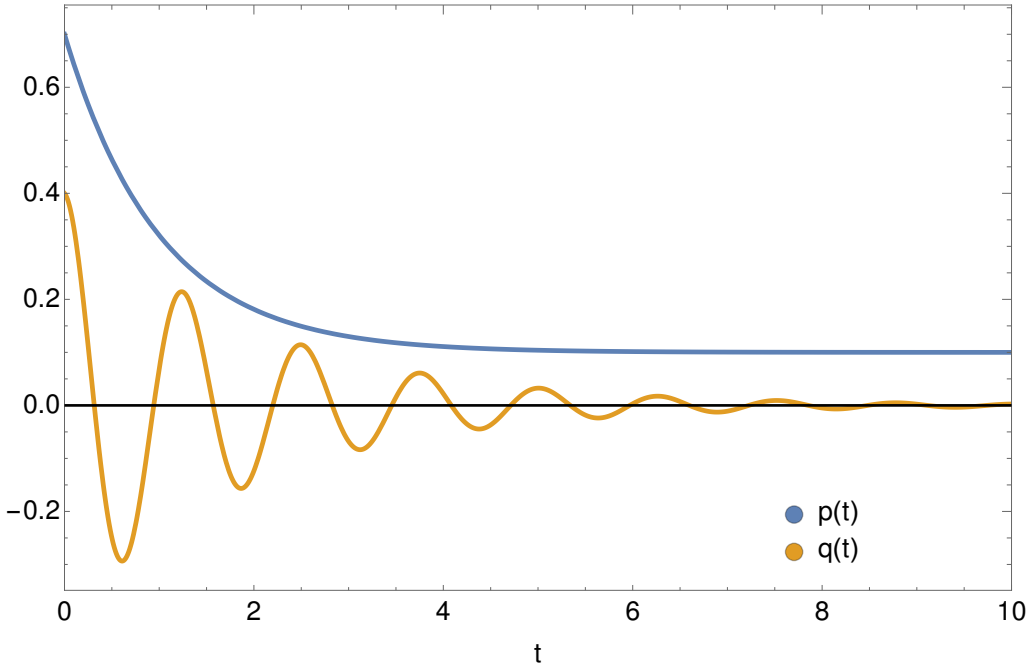

Figure 2.2: Evolution of the populations $p(t)$ and coherence $q(t)$ in the amplitude damping example. One can see the exponential decrease in $q(t)$ and the alteration in $p(t)$. Parameters used: $q_0 = 0.4, \Omega = 5, \gamma = 1, p_0 = 0.5, f = 0.1$.

These two examples provide us with a glance of the dynamics of systems evolving according to the Lindblad master equation, as well as how environment interactions may affect these systems. To our particular implementation, the vectorization procedure is quite important, as it will be used in the treatment of more complex systems which interest us. After understanding this key concept, we shall revisit the amplitude damping example using it.

2.2 Vectorization

The vectorization can be seen intuitively as a mapping procedure that takes a certain Hilbert Space and maps it to another one. In a more useful way, it turns a projector $|s_i\rangle\langle r_i|$ into a ket $|s_i r_i\rangle$ and generically, an operator into a vector, as the name implies. This is done in order to make it possible to use the tensor network techniques, all of which will be discussed in detail later 4. The following discussion is based around Ref.[17]. In

matrices, vectorizing is as simple as stacking columns:

$$\text{vec}\begin{pmatrix} a & b \\ c & d \end{pmatrix} = \begin{pmatrix} a \\ c \\ b \\ d \end{pmatrix}. \tag{2.14}$$

And for any three matrices A, B, C, it is true that

$$\text{vec}(ABC) = (C^T \otimes A)\text{vec}(B). \tag{2.15}$$

This is an important property of the vectorization operation, which can be directly verified. We'll make use of it extensively throughout this work, with the objective of reaching a vectorized version of ρ, since Eq.2.15 conveniently fits into the format of the operators in the Lindblad master equation, as in 2.10, although it is smart to insert an identity matrix around ρ in some cases.This leads us to three instances,

$$\begin{aligned} \text{vec}(A\rho C) &= (C^T \otimes A)\text{vec}(\rho), \\ \text{vec}(A\rho) = \text{vec}(A\rho I) &= (I \otimes A)\text{vec}(\rho), \\ \text{vec}(\rho C) = \text{vec}(I\rho C) &= (C^T \otimes I)\text{vec}(\rho). \end{aligned} \tag{2.16}$$

For instance, regarding the unitary term in the master eq., we have that

$$\text{vec}([H, \rho]) = (I \otimes H - H^T \otimes I)\text{vec}(\rho). \tag{2.17}$$

Additionally, the vectorization would read, regarding vectorial spaces, as follows

$$|i\rangle\langle j| \rightarrow |j\rangle \otimes |i\rangle . \tag{2.18}$$

And if we decompose ρ in a canonical orthonormal basis, we can represent it with a tensor decomposition:

$$\rho = \sum_{ij} \rho_{ij} |j\rangle \otimes |i\rangle . \tag{2.19}$$

Sequentially, regarding the master equation, it is possible to encompass the entire dynam-

ics in a *super-operator* $\mathcal{L}$, the Liouvillian. By doing this, defining

$$\frac{d\rho}{dt} = -i[H, \rho] + D(\rho) = \mathcal{L}(\rho), \tag{2.20}$$

we'd get

$$\frac{d\rho}{dt} = \mathcal{L}(\rho). \tag{2.21}$$

And by means of vectorization, we reach

$$\frac{d\rho}{dt} = \mathcal{L}(\rho) \longrightarrow \frac{d\left|\rho\right\rangle}{dt} = \hat{\mathcal{L}}\left|\rho\right\rangle, \tag{2.22}$$

and after that, this problem can be seen as

$$\frac{d\left|\rho(t)\right\rangle}{dt} = \hat{\mathcal{L}}\left|\rho(t)\right\rangle \longrightarrow \left|\rho(t)\right\rangle = e^{\hat{\mathcal{L}}t}\left|\rho(0)\right\rangle. \tag{2.23}$$

If we, then, take λ_k to be the eigenvalues of $\mathcal{L}$ and take $\left|x_k\right\rangle$ and $\left\langle y_k\right|$ as respectively, the right and left normalized eigenvectors, we have

$$\begin{aligned} \mathcal{L}\left|x_k\right\rangle &= \lambda_k\left|x_k\right\rangle, \\ \left\langle y_k\right|\mathcal{L} &= \left\langle y_k\right|\lambda_k. \end{aligned} \tag{2.24}$$

Let's say both of these have dimension d. This leads us to

$$\mathcal{L} = \sum_{k=0}^{(d^2-1)} \lambda_k \left|x_k\right\rangle\left\langle y_k\right|. \tag{2.25}$$

And so, the solution of 2.23 can be written as

$$\left|\rho(t)\right\rangle = \sum_{k=0}^{(d^2-1)} e^{\lambda_k t}\left|x_k\right\rangle\left\langle y_k|\rho(0)\right\rangle. \tag{2.26}$$

2.3 Properties of the Liouvillian and relaxation to the steady state

It is important to look at the properties of the Liouvilian.By naively trying to solve Eq.2.23 as an eigenvalue/eigenvector problem, one may not obtain good results.

In the case of one-dimensional spin chains, for instance, the steady-state is unique, and therefore, two interesting properties stand. One of the eigenvalues contained in λ_0 must be zero, and the others must be negative in order to obtain a stable solution. Together with that, relating λ_0 to the corresponding eigenvector, it must be true that

$$\langle y_0 \,|\, \rho(0) \rangle = 1, \tag{2.27}$$

and therefore, we have that

$$|y_0\rangle = \text{vec}(I)^T. \tag{2.28}$$

By plugging 2.28 back into 2.26, one can see that the steady-state is given by $|x_0\rangle$, and we can re-write 2.26 with that in mind,

$$|\rho(t)\rangle = |\rho_{ss}\rangle + \sum_{k=1}^{(d^2-1)} e^{\lambda_k t} \, |x_k\rangle\langle y_k|\rho(0)\rangle \,, \tag{2.29}$$

and note that as the other eigenvalues $\lambda_k, k > 1$ are negative, $\rho(t)$ converges to ρ_{ss} as t increases.

Looking back at 2.23, in the steady-state we have that $\frac{d|\rho(t)\rangle}{dt} = 0$, which leads us to

$$\mathcal{L} \, |\rho_{ss}\rangle = 0, \tag{2.30}$$

confirming the fact that the steady-state is the eigenvector with eigenvalue 0 of the Liouvillian.

Indeed, the matrices after vectorization will have higher dimensions that those in the initial example 2.1.2, but they are sparse, and using specialized algorithms may lead to satisfying results. Such approach is then used to compute the steady-state, and, as a matter of fact, is the most standard, but may become prohibitive depending on the system.

The reason for that is that the system might, during its evolution to the steady-state, pass through highly entangled states, extending itself over the Hilbert Space, which might be, depending on the size of the system, huge. This compromises the reliability of this particular method of simulation, since the convergence is not always assured in a reasonable amount of computational time, a problem we shall deal with later, in Sec.4.4.3. For now, let us revisit the amplitude damping example, using the vectorization procedure.

2.4 Vectorized example - amplitude damping

We shall now revisit the example done in 2.1.2, but using vectorized analogs of operators and density matrix. Indeed, as we had 2.8, by using the identities derived back in 2.16, we can now perceive the master equation as

$$\frac{d\ \mathrm{vec}(\rho)}{dt} = \mathcal{L}\ \mathrm{vec}(\rho), \tag{2.31}$$

where

$$\hat{\mathcal{L}} = H + \gamma(1-f)D[\sigma_-] + \gamma f D[\sigma_+], \tag{2.32}$$

with

$$\hat{H} = -i\frac{\Omega}{2}\Big[I \otimes \sigma_z - \sigma_z^T \otimes I\Big], \tag{2.33}$$

and

$$\hat{D}[\sigma_+] = \Big[\sigma_+^T \otimes \sigma_- - \frac{1}{2}\big(I \otimes (\sigma_+\sigma_-) + (\sigma_+\sigma_-)^T \otimes I\big)\Big], \tag{2.34}$$

$$\hat{D}[\sigma_-] = \Big[\sigma_-^T \otimes \sigma_+ - \frac{1}{2}\big(I \otimes (\sigma_-\sigma_+) + (\sigma_-\sigma_+)^T \otimes I\big)\Big]. \tag{2.35}$$

Note that we have taken vec(ρ) out of the mess of operators, and left it to be treated after the operations with matrices are dealt with. If we recall the same density matrix as 2.12, we have it as

$$\mathrm{vec}(\rho) = \begin{pmatrix} p \\ q^* \\ q \\ 1-p \end{pmatrix}, \tag{2.36}$$

and by calculating $\mathcal{L}$ with 2.32 and applying it back to $|\rho\rangle$ 2.36 one is able to derive, as before, the functions p and q as in 2.13

$$\boxed{\text{vec}(\rho) = \begin{pmatrix} p_0 e^{-\gamma t} + f(1 - e^{-\gamma t}) \\ q_0^* e^{(i\Omega + \gamma/2)t} \\ q_0 e^{-(i\Omega + \gamma/2)t} \\ 1 - p_0 e^{-\gamma t} + f(1 - e^{-\gamma t}) \end{pmatrix}} \tag{2.37}$$

Chapter 3

Open quantum spin chains

3.1 One dimensional quantum spin chains

Spin chains have been widely studied since they can show interesting physical properties, all the while being relatively simple regarding the physics. In a spin chain, electrons interact along the lattice according to Pauli exclusion principle and Coulomb repulsion. Tthese two factors can be seen as a competition between an exchange interaction and hopping between sites. These models are regarded as good toy models as they account for a myriad of properties. In this context, we have studied the variation in which there are baths coupled one dimensional chains. We now shall make a quick review of these models and discuss some results in the literature regarding its properties.

3.1.1 The XXZ model

In this work we have studied the spin-1/2 XXZ chain, whose particular Hamiltonian for a chain composed of N sites reads[1]:

$$\mathcal{H} = \sum_{i=1}^{N} \tau(\sigma_i^x \sigma_{i+1}^x + \sigma_i^y \sigma_{i+1}^y + \Delta \sigma_i^z \sigma_{i+1}^z) + \sum_{i=1}^{N} h\sigma_i, \tag{3.1}$$

where $\sigma_i^{x,y,z}$ are the Pauli matrices related to the site i. The parameter Δ relates to the anisotropy along the z axis (which gives this model the XXZ name). By setting, for instance, $\Delta = 1$, we recover the Heisenberg original XXX model, and by setting $\Delta = 0$, we get the so called XX model. The parameter h is the magnetic field acting on site i. And

[1] In this work we shall set both the Planck Constant ($\hbar$), Boltzmann constant (k_B) and Bohr Magneton (μ_B) to 1.

τ corresponds to the coupling between nearest neighbor sites. Without loss of generality, we henceforth set $\tau = 1$, which therefore fixes the energy scale of the problem.

By exploring symmetries related to these chains, one is able to derive many interesting properties. They are summarized in phase diagram of the system, found in figure 3.1.

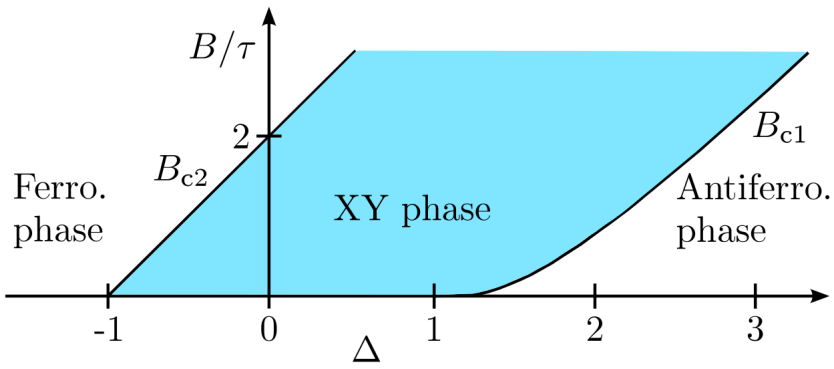

Figure 3.1: Phase diagram of the XXZ model 3.1. Taken from Ref.[11]. Here B is the magnetic field, which was labelled h in Eq.3.1.

If the magnetic field is set to zero, then the system goes from ferromagnetic at $\Delta = -1$, to antiferromagnetic at $\Delta = 1$. In the ferromagnetic phase the system is fully polarized along the z axis, as $|\uparrow\uparrow ... \uparrow\rangle$ or $|\downarrow\downarrow ... \downarrow\rangle$. These are degenerate as there's no preferencial direction to which the spins will be set to. For the antiferromagnetic case, the system ground state can be studied via the Bethe Ansatz method [7]. For $\Delta \in [-1, 1]$ in between -1 and 1, the system is in the paramagnetic state, which has no preferred order. Both the ferromagnetic and antiferromagnetic states are usually gapped, i.e., there is an energy cost associated with creating an excitation. The same is not true for the paramagnetic phase, which is gapless.

This behaviour changes with the presence of a magnetic field, since the spins have a tendency to align parallel to it. There's a critical field B_c that separates ordered and disordered phases, and it increases monotonically with Δ. The value B_{c1} is the critical field that separates the antiferromagnetic phase and the paramagnetic phase [18]. Aditionally, the critical field that separates the paraferromagnetic and ferromagnetic case is given by $B_{c2} = 2\tau(1 + \Delta)$ [11].

3.2 Open systems - environments

Even though the closed scenario (i.e. no environment coupled to the system) might be relatively simple to simulate when taking into account few electrons, it rapidly devolves into complicated many-body problems. It becomes even more complicated when one tries to take into account the interaction between the chain and thermal baths coupled to certain sites. An example can be seen in Fig.3.2.

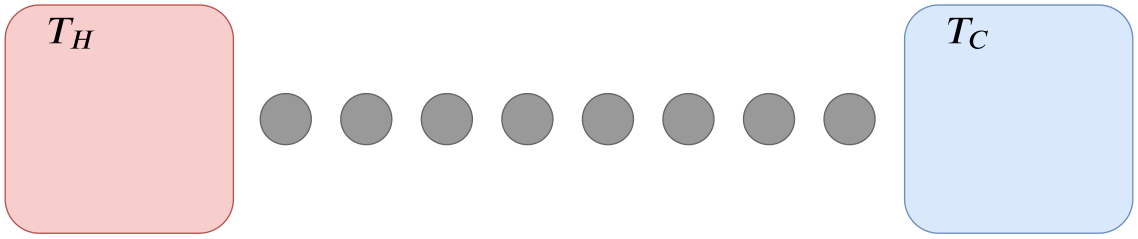

Figure 3.2: A one-dimensional chain where hot and cold baths are coupled to the first and last sites.

One can picture each bath as a multitude of spins set in the same manner, which interact with one or more elements of the chains. Here we do this using the concept of Lindblad master equations described in Eq.3.2. In particular, we focus on the so-called local master equations, which are obtained by using local dissipators acting only on a single site, which we assume have the form:

$$D_j(\rho) = \gamma f_j \left[\sigma_j^- \rho \sigma_j^+ - \frac{1}{2}\sigma_j^+\sigma_j^+\rho - \frac{1}{2}\rho\sigma_j^+\sigma_j^-\right] + \gamma(1-f_j)\left[\sigma_j^+\rho\sigma_j^- - \frac{1}{2}\sigma_j^-\sigma_j^+\rho - \frac{1}{2}\rho\sigma_j^-\sigma_j^+\right], \tag{3.2}$$

where the γ parameter relates to the coupling strength between the system and the bath. The f_j terms relate to the temperature in which the baths are held, being related to a reservoir inverse temperature β by $f = \tanh(\beta)$, such that for $f = 1$, $T = 0$ and for

$f = 0, T \to \infty$. As before, if we set the chain to be an XXZ, then the Hamiltonian is

$$\mathcal{H} = \sum_{i=1}^{N}(\sigma_i^x\sigma_{i+1}^x + \sigma_i^y\sigma_{i+1}^y + \Delta\sigma_i^z\sigma_{i+1}^z) + \sum_{i=1}^{N} h\sigma_i, \tag{3.3}$$

For instance, when looking at a one-dimensional spin chain, with baths coupled to the first and last sites, the Lindblad Equation takes this form

$$\frac{d\rho}{dt} = -i[\mathcal{H}, \rho] + D_1(\rho) + D_N(\rho) \equiv \mathcal{L}\rho, \tag{3.4}$$

where $\mathcal{L}$ stands for the Liouvillean Super Operator, which encompasses the entire dynamics of the system. This particular setup is interesting to our study on transport among the chain, dictated by the baths coupled to each end of it.

3.3 Transport regimes on one dimensional systems

In this section we derive the operators that relate to the transport throughout the system in the case of spin-1/2 XXZ chain. This is done in order to quantify how the environment affects the chain. We also discuss some results in the literature, in which the transport is mapped regarding different parameters.

The spin current for the model can be constructed by looking at the evolution of the internal sites of the chain ($k = 2, \ldots, N-1$). Since the dissipator only acts on sites 1 and N, it then follows that

$$\frac{d\sigma_k^z}{dt} = i[H, \sigma_k^z] = J_{k-1} - J_k, \tag{3.5}$$

where H is the Hamiltonian defined in Eq.3.1. Using only the algebra of the Pauli matrices leads to

$$J_k = 2\langle\sigma_k^x\sigma_{k+1}^y - \sigma_k^y\sigma_{k+1}^x\rangle. \tag{3.6}$$

Another important quantity studied is the magnetization at each site. It is given by

$$M_k = 2\langle\sigma_k^z\rangle, \tag{3.7}$$

Both Eq.3.6 and Eq.3.7 attain for the transport properties of the system. As we now

discuss, depending on Δ, γ and the f_i, the chain can present different transport regimes.

3.3.1 Ballistic behavior for $\Delta < 1$

By setting the anisotropy term $\Delta = 0$, the XX chain system is recovered. For the setup in 3.2, that is, coupling a bath to the first and last site of the chain, we can reach an exactly solvable prospect with the same Hamiltonian as 3.1 but with $\Delta = 0$. This was first shown in Ref.[19]. They found that the current has the form

$$J = \frac{\gamma}{1+\gamma^2}\frac{f_1 - f_L}{2}, \tag{3.8}$$

And the magnetization is

$$M = \frac{f_1 + f_L}{2}, \tag{3.9}$$

with γ being the coupling term, as in 3.1, and f_1 and f_L relating to the temperature of the baths interacting with site 1 and L.

This result therefore allows us to conclude that for $\Delta = 0$, the transport regime is ballistic, as the the values of flux 3.8 and magnon density 3.9 are independent on the chain size. The same holds true for $\Delta < 1$; the flux does not depend on the size of the chain [20].

3.3.2 Diffusive behavior for $\Delta > 1$

For values of Δ larger than one, the regime is called diffusive, in which the transport properties depend on the size of the chain according to $J \sim 1/N$. This has been studied by numerous works, and we focus on the discussion made at [21]. The Hamiltonian is reformulated to be close to the Ising Hamiltonian,

$$H = \sum_{j=1}^{n-1} \epsilon(\sigma_j^x \sigma_{j+1}^x + \sigma_j^y \sigma_{j+1}^y) + \sigma_j^z \sigma_{j+1}^z, \tag{3.10}$$

with $\epsilon = 1/\Delta$.

By expanding up to order ϵ^2, it is possible to derive the lowest order correction in the

NESS. This is done by considering an expansion of the form:

$$\rho = \frac{1}{2^N}(I + \mu\rho_0 + \mu\epsilon\rho_1 + \mu\epsilon^2\rho_2 + ...). \tag{3.11}$$

One can derive linear equations for ρ_0, ρ_1, ρ_2. Interesting results regarding transport arise.

The authors show that, if the average magnetization profile is linear, the spin current scales as $1/N$, which means that the transport throughout the chain is diffusive. It is also possible to derive a diffusion constant D,

$$D = 2.95/\Delta, \tag{3.12}$$

and it is noted that this agrees nicely with numerical results (Fig.3.3).

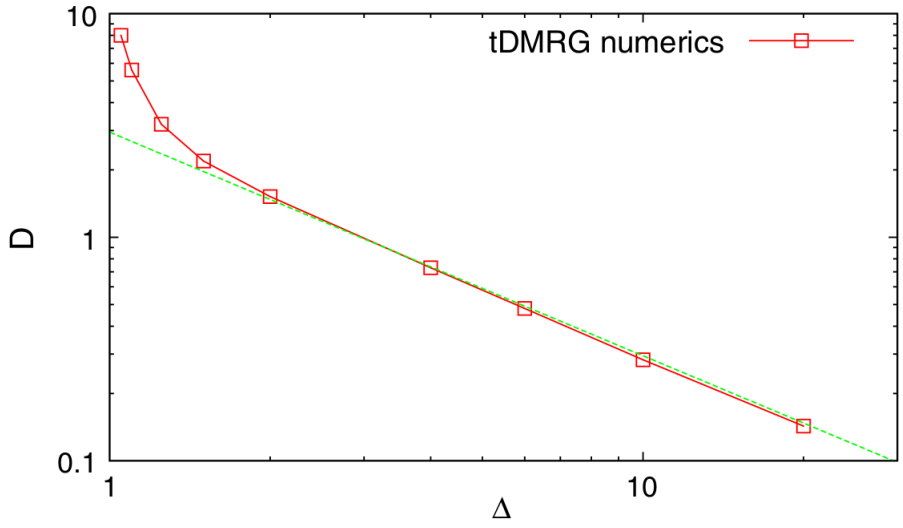

Figure 3.3: Noted dependence of the diffusion constant 3.12 related to Δ. Taken from Ref.[21].

3.3.3 Anomalous transport for $\Delta = 1$

The case $\Delta = 1$ is special and exhibits anomalous transport. The transport in this case becomes sensitive to the other parameters, h, γ and f. Depending on the values of these parameters, one may find sub-diffusive transport, with $J \sim 1/N^2$ [22] as well as super-diffusive transport, $J \sim 1/\sqrt{N}$ [21]. The complete phase diagram of this model is still unknown and was part of the initial motivation for this dissertation.

Regarding Eq.3.2, if we set $f_1 = 1$ and $f_N = 0$, and plug it back into Eq.3.4, then one of the baths is a perfect magnon source, pumping in magnons in and out of the system at the rate γ whereas the other acts as a perfect magnon sink, absorbing magnons at a rate γ. In this case, it is possible to look at the problem analytically, with the aid of a *matrix product state*(MPS) solution, as first started in Ref.[23] and later extended in Ref.[22]. By making use of matrix product states, the paper found an interesting analytical result for the spin flux between neighboring sites i and $i+1$, given by

$$J_i = \frac{2\gamma}{\gamma^2 + h^2} \frac{Z(N-1)}{Z(N)}, \tag{3.13}$$

in which $Z(N) = (B^N)_{0,0}$ is calculated exponentiating the matrix

$$(B)_{k,l} = 2|p-k|^2 \delta_{k,l} + l^2 \delta_{k,l-1} + |2p-l|^2 \delta_{k,l+1}, \tag{3.14}$$

where k and l stand for the element indices and p is given by

$$p = \frac{i}{2(\gamma - ih)}. \tag{3.15}$$

Using this result, the relation between flux and chain size was found to go with $J \sim 1/N^2$, which is an interesting result notable in Fig.3.4.

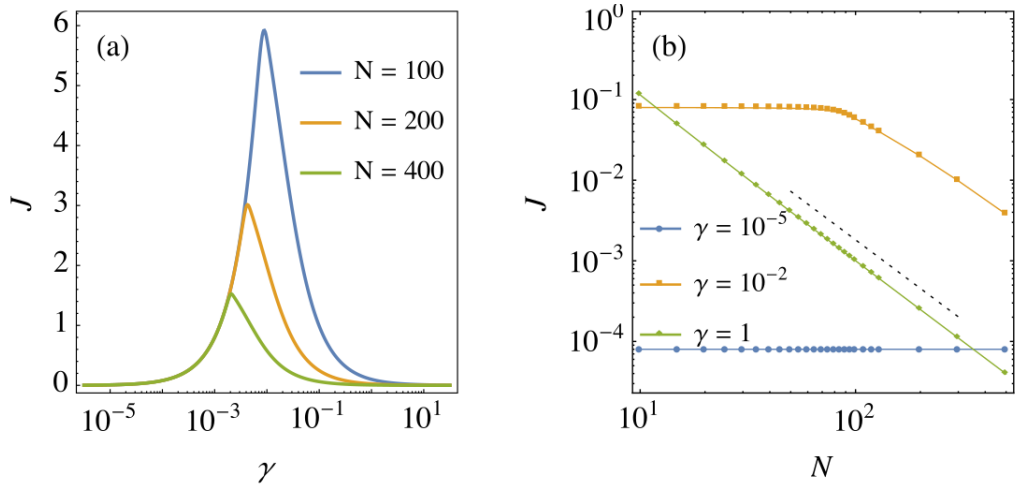

Figure 3.4: An interesting composition in which the flux can be seen to change from constant to dependent on N, after a certain threshold. Taken from Ref.[22]

.

The results up until this point provide excellent benchmarking prospects for the simulations we shall discuss in the next chapters, given that the baths are perfect magnon sources.

3.4 The problem at hand

The anomalous transport exhibited by the Heisenberg model ($\Delta = 1$) is extremely interesting and still poorly understood. For $\Delta < 1$ or $\Delta > 1$ the system behaves, respectively, ballistically or diffusively, independently of the other parameters. But for $\Delta = 1$ the results in Refs.[20] and [21] show that the regime may change depending on the other parameters in the model. Moreover, the transport is neither ballistic nor diffusive, but rather sub-diffusive or super-diffusive. Understanding this interesting effect was part of the motivation for this dissertation.

Tackling this problem, however, is numerically challenging. The damping rate γ was found in Ref.[21] to play a critical role in the transport properties, specially when $\gamma \ll 1$. In contrast, practically all numerical studies done so far with this model have taken an arbitrary value $\gamma = 1$, imagining that this was unimportant. Numerical studies of this model using tensor networks, as will be described in the next chapter, usually make use of a time-dependent evolution to reach the steady-state. For low values of γ, however, extremely long times may be necessary, making the simulations inviable. The method implemented in this dissertation was devised precisely to circumvent this difficulty.

To summarize, therefore, simulating the case $\Delta = 1$ for different choices of h, γ and f_i constituted the main physical objective of this dissertation.

Chapter 4

Tensors and tensor networks

4.1 The structure of the Hilbert space

Usually, quantum physics problems are studied using the concept of Hilbert space, which is a rather abstract concept, although being mathematically well defined. In general lines, the Hilbert Spaces are generalizations of euclidean spaces, and take into account vector algebra for arbitrarily large dimensions. This is partly due to the fact that quantum states are seen as superpositions of states. This fits nicely into the structure of a tensor, which is the reason we choose to represent physical states with the help of tensor networks.

For a many-body problem, as we've discussed, the associated Hilbert space grows fast, and therefore demands a lot of memory to be represented completely.

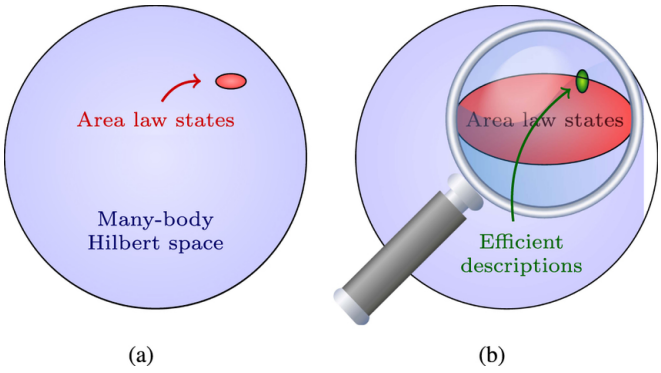

Figure 4.1: In a Hilbert space related to a certain system, even though it might be quite extense, only small portions contain the physical states. Taken from Ref.[24].

However, despite being extremely large, not all of Hilbert space is typical; that is, most physical states actually occupy only small regions of the full space (see Fig.4.1). And therefore, it is possible for approximations to be efficient descriptions of the system

without having to store it entirely [24]. This is the foundation behind the matrix product state ansatz, as well as the following density matrix renormalization technique, which aims to control the growth of the Hilbert space in a educated guess, as we'll show.

4.2 Matrix product states

Before starting on to the matrix product states formulation, it is convenient to have a quick look at the tensor entity. Tensors are sophisticated tools with a wide range of applications, ranging from the cosmology calculations to the topological abstract mathematics to quantum physics, with its use being especially computer friendly, in an era where simulation power is key.

As so, in this work, the tensors, which are themselves generalizations of vectors in arbitrarily large spaces, are generalized yet again, in what are called *tensor networks*. This attains for huge gain in computational power, which is very welcome.

This is due to the fact that, in the quantum framework, the many body problem presents even more of a challenge than its classical counterpart, as the Hilbert Space related to these systems scales up exponentially to the quantity of individual particles being simulated.

What differentiates between tensors and scalars are the **indices**. The simplest of tensors shall have one index, and it is an appropriate moment to introduce the diagrams which we'll use to illustrate the tensors. A rank-1 tensor A with a single index x_1 can be seen diagrammatically as follows in Fig.4.2.

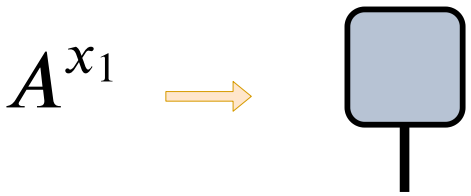

Figure 4.2: Simple tensor diagram of a rank-1 tensor. The node is index is depicted by the black dash

We can make it so that A now has two indices instead of one, x_1, x_2, as in Fig.4.3.

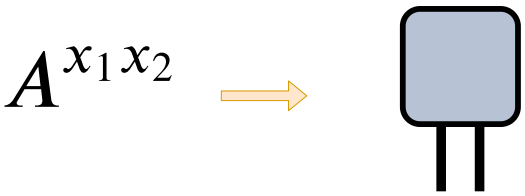

Figure 4.3: Simple tensor diagram of a rank-2 tensor.

Note that this would add another line sticking out of the tensor container, which means exactly that, another index. For a more interesting example, say we can re-write our toy-tensor A as two different tensors, $B^{x_1}_{y_1}$ and $B^{x_2}_{y_1}$, which would lead us to the diagram in Fig.4.4.

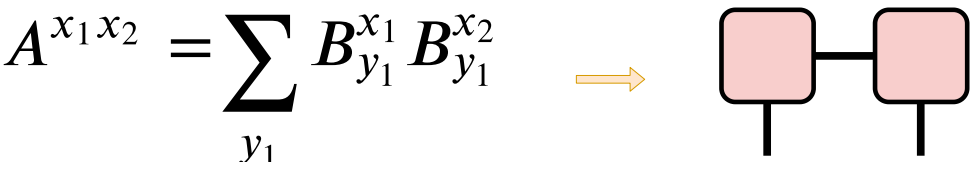

Figure 4.4: Simple tensor diagram of a rank-2 tensor decomposition into two rank-2 tensors.

As we contract over the y_1 index, we get A back from that. This example illustrates the fundamental idea behind tensor networks; namely, representing high-rank tensors as objects with internal structure, composed of contractions of lower order tensors.

Let us now consider a physical system composed (for concreteness) of N spin 1/2 particles. The most general pure state of this system may be written as

$$|\Psi\rangle = \sum_{\sigma_1,\ldots,\sigma_L} \psi_{\sigma_1,\ldots,\sigma_L} |\sigma_1,\ldots,\sigma_L\rangle, \tag{4.1}$$

for some set of coefficients $\psi_{\sigma_1,\ldots,\sigma_L}$. The connection with tensors now comes from interpreting the vector of coefficients $\psi_{\sigma_1,\ldots,\sigma_L}$ as a rank-L tensor.

Regarding to the particular simulation of quantum many body, the key concept is the Matrix Product State (MPS), which will work as an ansatz. The set of coefficients in 4.1

would be written as a set of tensors $A^{\sigma_1}_{x_1} A^{\sigma_2}_{x_1,x_2} ... A^{\sigma_N}_{x_{N-1}}$, as in

$$|\Psi\rangle = \sum_{\substack{\sigma_1,\sigma_2,...\sigma_N \\ x_1,x_2,...,x_{N-1}}} A^{\sigma_1}_{x_1} A^{\sigma_2}_{x_1,x_2} ... A^{\sigma_N}_{x_{N-1}} |\sigma_1\sigma_2...\sigma_N\rangle , \tag{4.2}$$

Now there's exactly the same example, just more complex, as we're dealing with a physical state $|\Psi\rangle$, and in the same way, can be seen as a simple diagram [16] depicted in Fig.4.5.

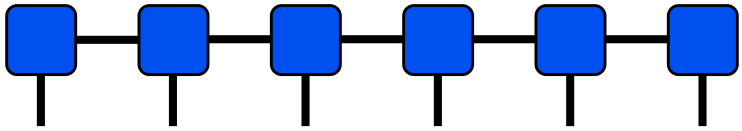

Figure 4.5: Pictoric diagram of a MPS state $|\Psi\rangle$.

With the central light-blue nodes representing the Tensors and the information that's stored within, and with the black dashes representing the indices. As before, when connecting two nodes, that particular index is being summed over [10]. In this depiction, the *physical indices* $(\sigma_1, \sigma_2, ..., \sigma_N)$ are stick out without being summed over, while the internal MPS indices $(x_1, x_2, ..., x_{N-1})$

4.3 Matrix product operators

A similar thing can be said about any particular operators, which can be perceived as an Matrix Product Operator object (MPO), with the exact same structure, and one particularity, the number of indexes it has[10].

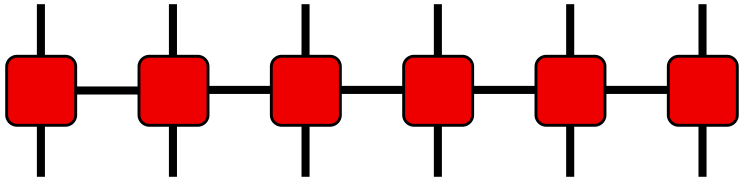

Figure 4.6: Pictoric diagram of a MPO operator $\mathcal{O}$.

An MPO will have the general structure

$$\mathcal{O} = \sum_{\substack{\sigma_1,...,\sigma_N \\ \sigma'_1,...,\sigma'_N \\ x_1,x_2,...,x_{N-1}}} W_{x_1}^{\sigma_1,\sigma'_1} W_{x_1,x_2}^{\sigma_2,\sigma'_2} ... W_{x_{N-1}}^{\sigma_N,\sigma'_N} \left|\sigma_1, ..., \sigma_N\right\rangle\left\langle\sigma'_1, ..., \sigma'_N\right|, \tag{4.3}$$

which is represented in Fig.4.6

Apart of the indices connecting over the nodes, the operator (for instance, the hamiltonian) associated with a system shall have twice the physical indexes in relation with the MPS that represents the system. This makes sense, as these indices will be summed over when calculating, for instance, an expected value.

This specific diagramatization scheme makes it especially intuitive to perceive the calculations of expected values of operators, norms of quantum states and so on, as contracting over indexes would just represent linking up black dashes in the same way. In this sense, this also conveys the dimensionality of the result by looking at the final count of dashes sticking out, as a non-contracted index. For instance, two of them sticking out would mean the final result to be a rank-2 tensor.

4.4 Tensor network methods

Since the original work by Steven White [13], techniques derived from Renormalization Groups formalism while using the Density Matrix have become the major methods for the simulation of dynamics of Strongly Correlated Systems. This wasn't always the case, and some other methodologies are worth discussing, since they do provide valuable tools as well.

4.4.1 Exponential time evolution

The usual setup derived from Eq.2.23 requires evolving the initial state of the given system by exponentiating the Liouvillean and applying it over the initial state $|\rho(0)\rangle$ iteratively, as in

$$e^{\mathcal{L}(t_0+\Delta_t)} |\rho(0)\rangle = |\rho(t_1)\rangle \dots \tag{4.4}$$

Exponentiating a matrix and applying it onto a vector is not a quite demanding task by itself, but some problems may surface while trying to get to the steady state, since the highly non-local aspects of the systems of interest may deem the simulations unviable, as the Hilbert space may easily and surely grows larger and larger.

4.4.2 Trotter time evolution

A workaround for specific scenarios, for instance, when there's only at most nearest-neighbour interaction, are the array of techniques related to Time Evolving Block Decimation, whose most relevant branch is the Trotter time evolution, which samples the name from the Suzuki-Trotter expansion. This method works mostly when the entanglement present in the system is controlled and limited, as this, in turn, controls the Hilbert Space dimension associated to the problem. In this framework, one might attempt a first order Trotter decomposition by breaking up the Hamiltonian in local parts, which act on one site at a time, as in

$$e^{-iHt} = e^{-ih_1 t/2} \dots e^{-ih_L t/2} e^{-ih_{(L-1)} t/2} \dots e^{-ih_1 t/2} + O(t^3). \tag{4.5}$$

The error of this aproximation is due to the non-commutativity of the local parts of the Hamiltonians, and it will be of order t^3. After breaking the Hamiltonian down to local parts, it can be used to do a time evolution that is simpler to compute. This method can be extended to Hamiltonians with finite range interactions. This is further discussed in Ref.[25].

4.4.3 Tensor networks approach to ground state convergence

Althought being interesting methods, the limitations of each can become prohibitive and hinder simulation efforts. A variational setup, then, becomes useful to deal with these eigenvalues-eigenvectors problems. For a simple example, say one desires to find the ground state energy associated with a certain Hamiltonian H and a certain state Ψ, fos instance, composed of 4 sites.

$$E = \frac{\langle \Psi | \, H \, | \Psi \rangle}{\langle \Psi | \Psi \rangle}. \tag{4.6}$$

We want to calculate $\langle\Psi|\, H\, |\Psi\rangle$, to a 4-site Ψ, where

$$|\Psi\rangle = \sum_{\substack{\sigma_1,\sigma_2,\\ \sigma_3,\sigma_4}} A^{\sigma_1} A^{\sigma_2} A^{\sigma_3} A^{\sigma_4} \,|\sigma_1,\sigma_2,\sigma_3,\sigma_4\rangle\,, \tag{4.7}$$

$$= \sum_{\substack{\sigma_1,\sigma_2,\\ \sigma_3,\sigma_4}} \sum_{a_1,a_2,a_3} A^{\sigma_1}_{a_1} A^{\sigma_2}_{a_1,a_2} A^{\sigma_3}_{a_2,a_3} A^{\sigma_4}_{a_3} \,|\sigma_1,\sigma_2,\sigma_3,\sigma_4\rangle\,. \tag{4.8}$$

To aid us, we insert (non-physical) indices connecting each of the matrices associated with each site with the neighbouring sites matrices. A representation of it is depicted in Fig.4.7.

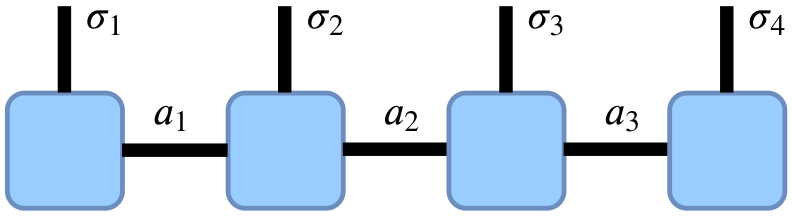

Figure 4.7: MPS representation of a 4-site state $|\Psi\rangle$.

As for the Hamiltonian H, we have

$$H = \sum_{\substack{\sigma_1,\sigma_2,\sigma_3,\sigma_4\\ \sigma'_1,\sigma'_2,\sigma'_3,\sigma'_4}} W^{\sigma_1,\sigma'_1} W^{\sigma_2,\sigma'_2} W^{\sigma_3,\sigma'_3} W^{\sigma_4,\sigma'_4} \,|\sigma_1,\sigma_2,\sigma_3,\sigma_4\rangle\langle\sigma'_1,\sigma'_2,\sigma'_3,\sigma'_4|\,, \tag{4.9}$$

which can be represented as a Matrix Product Operator, found in Fig.4.8.

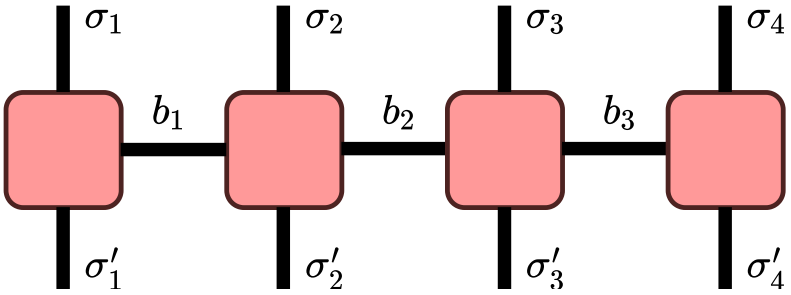

Figure 4.8: MPO representation of a 4-site operator. In this case, a Hamiltonian.

This Hamiltonian can be written more compactly as

$$H = \sum_{\sigma,\sigma',b} W_{b_1}^{\sigma_1,\sigma_1'} W_{b_1,b_2}^{\sigma_2,\sigma_2'} W_{b_2,b_3}^{\sigma_3,\sigma_3'} W_{b_3}^{\sigma_4,\sigma_4'} \left|\sigma\right\rangle\left\langle\sigma'\right|. \tag{4.10}$$

And now, with both $\left|\Psi\right\rangle$ and H at hand, we're able to calculate $\left\langle\Psi\right| H \left|\Psi\right\rangle$.

$$\begin{aligned}\left\langle\Psi\right| H \left|\Psi\right\rangle = &\left[\sum_{\sigma} \left(A^{\sigma_1} A^{\sigma_2} A^{\sigma_3} A^{\sigma_4}\right)^{\dagger} \left\langle\sigma\right|\right] * \\ &\left[\sum_{\sigma',\sigma''} \left(W^{\sigma_1',\sigma_1''} W^{\sigma_2',\sigma_2''} W^{\sigma_3',\sigma_3''} W^{\sigma_4',\sigma_4''}\right) \left|\sigma'\right\rangle\left\langle\sigma''\right|\right] *. \\ &\left[\sum_{\sigma'''} \left(A^{\sigma_1'''} A^{\sigma_2'''} A^{\sigma_3'''} A^{\sigma_4'''}\right) \left|\sigma'''\right\rangle\right]\end{aligned} \tag{4.11}$$

By focusing solely on the coefficients, disregarding the deltas which would appear, we reach

$$\sum_{\sigma,\sigma'} \left(A^{\sigma_1} A^{\sigma_2} A^{\sigma_3} A^{\sigma_4}\right)^{\dagger} * \left(W^{\sigma_1,\sigma_1'} W^{\sigma_2,\sigma_2'} W^{\sigma_3,\sigma_3'} W^{\sigma_4,\sigma_4'}\right) * \left(A^{\sigma_1'} A^{\sigma_2'} A^{\sigma_3'} A^{\sigma_4'}\right). \tag{4.12}$$

And now, inserting the remaining indexes, there should be

$$\begin{aligned}\left\langle\Psi|H|\Psi\right\rangle = \sum_{\sigma,\sigma'} \sum_{a_1,a_2,a_3} \sum_{b_1,b_2,b_3} \sum_{c_1,c_2,c_3} &\left(A_{a_1}^{\sigma_1} A_{a_1,a_2}^{\sigma_2} A_{a_2,a_3}^{\sigma_3} A_{a_3}^{\sigma_4}\right)^{\dagger} * \\ &\left(W_{b_1}^{\sigma_1,\sigma_1'} W_{b_1,b_2}^{\sigma_2,\sigma_2'} W_{b_2,b_3}^{\sigma_3,\sigma_3'} W_{b_3}^{\sigma_4,\sigma_4'}\right) * \left(A_{c_1}^{\sigma_1'} A_{c_1,c_2}^{\sigma_2'} A_{c_2,c_3}^{\sigma_3'} A_{c_3}^{\sigma_4'}\right)\end{aligned}, \tag{4.13}$$

which can then be regrouped as

$$\begin{aligned}\left\langle\Psi|H|\Psi\right\rangle = \sum_{\substack{a_1,a_2,a_3,\\ b_1,b_2,b_3,\\ c_1,c_2,c_3}} &\left(\sum_{\sigma_1,\sigma_1'} A_{a_1}^{\sigma_1\dagger} W_{b_1}^{\sigma_1,\sigma_1'} A_{c_1}^{\sigma_1'}\right) * \left(\sum_{\sigma_2,\sigma_2'} A_{a_1,a_2}^{\sigma_2\dagger} W_{b_1,b_2}^{\sigma_2,\sigma_2'} A_{c_1,c_2}^{\sigma_2'}\right) * \\ &\left(\sum_{\sigma_3,\sigma_3'} A_{a_2,a_3}^{\sigma_3\dagger} W_{b_2,b_3}^{\sigma_3,\sigma_3'} A_{c_2,c_3}^{\sigma_3'}\right) * \left(\sum_{\sigma_4,\sigma_4'} A_{a_3}^{\sigma_4\dagger} W_{b_3}^{\sigma_4,\sigma_4'} A_{c_3}^{\sigma_4'}\right) *\end{aligned} \tag{4.14}$$

Finally, those are renamed as follows

$$\begin{aligned} L_{a_1,b_1,c_1} &= \sum_{\sigma_1,\sigma_1'} A_{a_1}^{\sigma_1} W_{b_1}^{\sigma_1,\sigma_1'} A_{c_1}^{\sigma_1'} \\ R_{a_3,b_3,c_3} &= \sum_{\sigma_4,\sigma_4'} A_{a_3}^{\sigma_4} W_{b_3}^{\sigma_4,\sigma_4'} A_{c_3}^{\sigma_4'} \end{aligned} . \tag{4.15}$$

By applying each local MPO to the respective MPS iteractively, we get the foundation of the variational setup. This procedure can be diagramatically seem as in Fig.4.9.

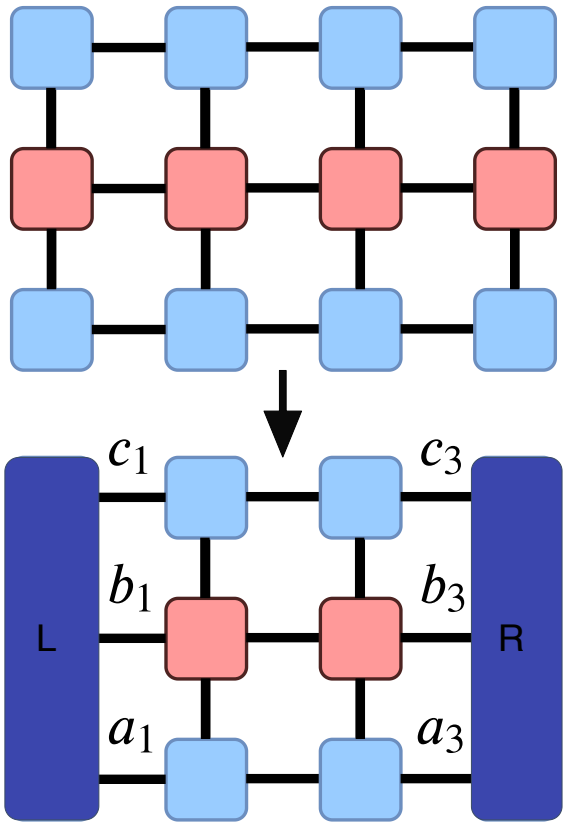

Figure 4.9: Diagrammatic representation of a step-by-step contraction of a 4-site operator expected value of the Hamiltonian. Note how no indices are left after fully contracting over all remaining indices.

By this exercise, we see how tensor treatment can be extremely useful for extensive calculations. Luckily, we're able to avoid such calculations by using the ITensor [16] package, which manages the indices in such operations, not only intuitively, but efficiently as well.

4.4.4 Variational principle

It is important to note how the MPS applications can be used to find the NESS of a quantum system. Let us suppose that a Hilbert space related to a certain system can be said to satisfy $\mathcal{H} : |i\rangle$ where $i = 0, ..., N-1$. We have that $|\Psi\rangle = \sum_\alpha \Psi_\alpha |\alpha\rangle$. The energy of the ground state should be upper bounded by

$$E_{gs} \leqslant \epsilon = \frac{\langle\Psi| H |\Psi\rangle}{\langle\Psi|\Psi\rangle}, \tag{4.16}$$

which can be re-written to look as

$$\epsilon\langle\Psi|\Psi\rangle = \langle\Psi| H |\Psi\rangle. \tag{4.17}$$

By taking the partial derivative in relation to $\Psi^\dagger_\alpha$, we get that

$$\left[\frac{\partial}{\partial\Psi^\dagger_\alpha}\right] \sum_{\alpha,\alpha'} \langle\alpha| H |\alpha'\rangle \Psi^\dagger_\alpha \Psi_{\alpha'} = \epsilon \sum_\alpha \Psi^\dagger_\alpha \Psi_\alpha, \tag{4.18}$$

which is equal to

$$\sum_{\alpha'} H_{\alpha\alpha'} \Psi_{\alpha'} = \epsilon \Psi_\alpha. \tag{4.19}$$

Finally

$$H |\Psi\rangle = \epsilon |\Psi\rangle. \tag{4.20}$$

4.5 The $\mathcal{L}^\dagger\mathcal{L}$ Technique

For our particular setup in our implementation, instead of minimizing the energy by looking at $H |\Psi\rangle = E |\Psi\rangle$, we look at the dynamics of the equation dictated by the Lindblad equation 3.4, in which we have a super-operator $\mathcal{L}$ conducting the evolution of a vectorized density matrix ρ.

$$\mathcal{L} |\rho\rangle = 0. \tag{4.21}$$

since $\mathcal{L}$ is not Hermitian, and thus its eigenvalues aren't necessarily real, 4.21 is unfit to simulations. However, by applying $\mathcal{L}^\dagger$ at both sides of 4.21, we get

$$\mathcal{L}^\dagger \mathcal{L} \left|\rho\right\rangle = 0. \tag{4.22}$$

This elegant idea was conceived in Ref.[12] and is extremely useful, as now the eigenvalues are not only real, but positive, and even more, the lowest one is zero. So when looking at simulation results, one is able to see it converging to zero, should it work properly. Therefore, we effectively know which eigenstate we're looking for, the one with eigenvalue zero.

Chapter 5

The density matrix renormalization group

This chapter will verse over the Density Matrix Renormalization Group algorithm, as well as our particular implementation for open quantum systems and the technical details on how the code works.

The initial implementations of the DMRG, when facing infinite-sized systems, dealt with the problem by analysing chains of increasing lengths, while truncating over the Hilbert Space so the dimension that represented the system wouldn't be prohibitive for the simulation. The key of the algorithm is this truncation, called decimation procedure. This lays on the assumption that the Hilbert space of the problem we are tacking is way larger than the space in which the dynamics of interest resides [10].

Originally, the implementation was carried out by starting from a two-site system which was divided naturally in two blocks, and then more sites were inserted between then, with the decimation procedure following after that. Schematically, this can be seen in figure 5.1.

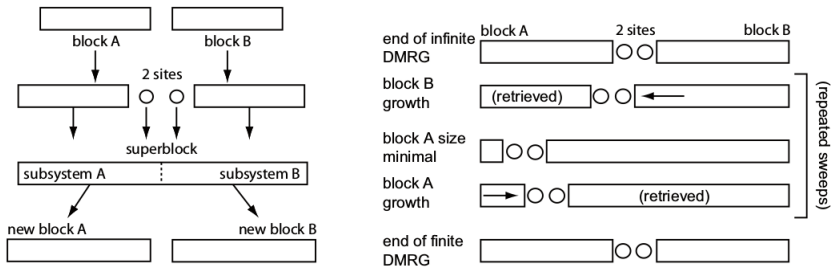

Figure 5.1: The decimation procedure represented schematically for infinite sized chains (left) and finite chains (right). Taken from Ref.[10]

Then, by looking at the ground-state energy of the chain, which is given by 4.6, by using an iterative sparse matrix eigensolver, one can find Ψ that minimizes the energy, effectively reaching a ground-state approximation. This configuration receives more sites, that are then taken into account for the calculation of the energy, and so on.

In its current state, such procedure is done by aid of an inconspicuous operation called the Singular Value Decomposition, or SVD, for short. The SVD is a purely algebraic tool, but it has a background in physics foundations, as it stands in the foundation of the Schmidt decomposition, and it relates with the entanglement entropy of bipartite systems. Let us take a look at how it works, and why it works.

5.1 Singular value decomposition

Any matrix T can be decomposed in 3, namely, $U, S, V^\dagger$, as

$$T = USV^\dagger. \tag{5.1}$$

Here, S is a diagonal positive matrix, that holds the singular values: $S = \text{diag}(\sigma_1.\sigma_2, \ldots, \sigma_r)$. The number of singular values is the Schmidt rank of the matrix T. The matrices to the left and to the right of S are usually called right and left orthogonal matrices as they satisfy, respectively $L^\dagger L = 1$, and R, $RR^\dagger = 1$. Diagrammatically, one can perceive the SVD as in Fig.5.2.

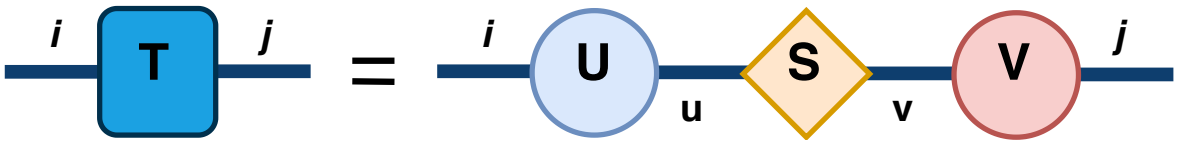

Figure 5.2: Diagrammatic representation of a SVD.

The SVD can be used to make low rank approximations of matrices. This is done by taking, for instance, a matrix T, $N \times N$, which will have N^2 entries, and instanciating it with vectors of dimension N, say, u and v. By taking the outer product $uv^\dagger$, which also has $N \times N$ entries, but is so that the entries are all specified by two tensors of size N, which effectively ranks down the initial matrix. A matrix given by outer product u and $v^\dagger$

is often called a rank-1[16]. For a simple example, may we look back at 5.1, which can also be seen as, in regard of each entry of matrix T,

$$T_{ij} = \sum_{\alpha=1}^{r} U_{i\alpha}\sigma_{\alpha}V^{*}_{j\alpha}. \tag{5.2}$$

The matrix T can be written in terms of two generic column vectors u_α and v_α, as in

$$T = \sum_{\alpha=1}^{r} \sigma_{\alpha}u_{\alpha}v^{\dagger}_{\alpha}, \tag{5.3}$$

which means that T has been decomposed as a sum of $r \leqslant N$ terms of rank-1 matrices. This can also yield a controlled approximation of T, in which we don't sum over all the singular values, but only a small number of them, so the problem is mapped into an approximation of diminished dimension. This can be extremely useful, since taking the sum over only one singular value, for instance, would map the N^2 elements in a $2N$ space.

5.1.1 Schmidt decomposition

We shall now run over a simple example of how the SVD can be applied on to quantum states study, and what does this approach tell us about entanglement. By considering two qubits, we have

$$|\Psi\rangle = \frac{c}{\sqrt{2}}(|00\rangle + |11\rangle) + \frac{d}{\sqrt{2}}(|01\rangle + |10\rangle), \tag{5.4}$$

where $|c|^2 + |d|^2 = 1$ for normalization. By a simple parametrization, we can write $c = cos(\phi/2)$ and $d = sin(\phi/2)$. By choosing either c or d, to be 1, we can recover the Bell states, which are, for instance, maximally entangled. By choosing $c = d = 1/\sqrt{2}$ we obtain a product state. We now express the state 5.4 as

$$|\psi\rangle = \sum_{ij} \psi_{ij}|i, j\rangle, \tag{5.5}$$

where the coefficients ψ_{ij} are now interpreted as a matrix,

$$\Psi = \frac{1}{\sqrt{2}} \begin{pmatrix} c & d \\ d & c \end{pmatrix}. \tag{5.6}$$

We now perform an SVD of this matrix Ψ. The matrices U and V turn out to be the same and are given by Haddamard gates:

$$U = V = \frac{1}{\sqrt{2}} \begin{pmatrix} 1 & 1 \\ 1 & -1 \end{pmatrix}. \tag{5.7}$$

The singular values matrix S, on the other hand, read:

$$S = \frac{1}{\sqrt{2}} \text{diag}(c + d, c - d). \tag{5.8}$$

Finally, this can be written in the Schimdt basis, as in

$$|\Psi\rangle = \frac{(c + d)}{\sqrt{2}} |{+}{+}\rangle + \frac{(c - d)}{\sqrt{2}} |{-}{-}\rangle . \tag{5.9}$$

This is quite interesting, as the SVD makes it easier to see how entanglement works in this particular system, way more easily to see as in 5.4. This calculation suggests that the SVD is a valuable tool to look at the entanglement of systems more easily, and therefore it helps us to re-write such problems so they are more easily treatable.

5.2 Tensor structures and the DMRG algorithm

As we have shown, the SVD is a powerful tool to treat physical systems. In our implementation, some particular properties are important. To understand these properties, let us consider, as before, a simple 1D system of N spins, and recall that a general state reads

$$\psi = \sum_{\sigma_1,...,\sigma_N} c_{\sigma_1,...,\sigma_N} |\sigma_1, ..., \sigma_N\rangle . \tag{5.10}$$

5.2.1 Left and right-canonical MPS ansatz

Looking at the coefficients $c_{\sigma_1,...,\sigma_N}$, we can write a $d \times d^{N-1}$ matrix Ψ using the vector of coefficients c, and by performing an SVD with such matrix, we would get

$$\Psi_{\sigma_1,...,\sigma_N} = c_{\sigma_1,...,\sigma_N} = U_{\sigma_1,a_1} S_{a_1 a_1} (V^\dagger)_{a_1,\sigma_2,...,\sigma_N}. \tag{5.11}$$

Decomposing U into d vectors L^{σ_1}, so that $L^{\sigma_1}_{a_1} = U_{\sigma_1,a_1}$ and by contracting S and $V^\dagger$ back together, we get

$$\Psi_{\sigma_1,...,\sigma_N} = c_{\sigma_1,...,\sigma_N} = \sum_{a_1}^{d'} L^{\sigma_1}_{a_1} \Psi_{a_1,\sigma_2,...,\sigma_N}. \tag{5.12}$$

This can now be repeated for the new set of coefficients $\Psi_{a_1,\sigma_2,...,\sigma_N}$ so that Ψ is entirely rewritten as matrices L, which can be summed over to recover Ψ, as in

$$c_{\sigma_1,...,\sigma_N} = \sum_{a_1,...,a_{N-1}} L^{\sigma_1}_{a_1} L^{\sigma_2}_{a_1,a_2} ... L^{\sigma_N}_{a_{N-1}}. \tag{5.13}$$

which is the decomposition of ψ into a matrix product state. We can rewrite our state as

$$\boxed{|\psi\rangle = \sum_{a_1,...,a_L} L^{\sigma_1} L^{\sigma_2} ... L^{\sigma_N} |\sigma_1, ..., \sigma_N\rangle} \tag{5.14}$$

As developed in Sec.4.2, this poses as a matrix product state representation of our initial state Ψ, in this case, we chose to keep all the *left-orthogonal matrices* resulting from repeated SVD's while contracting back the singular values with the righ-orthogonal parts of the decomposition. If we decompose a state completely using left-orthogonal matrices, we will call the matrix product state *left-canonical* as in Ref.[10]. Such matrices have the following property

$$\boxed{\sum_{\sigma_l} L^{\sigma_l \dagger} L^{\sigma_l} = I} \tag{5.15}$$

A similar argument can be made if we decompose Ψ into a succession of right-orthogonal matrices:

$$\Psi_{\sigma_1,...,\sigma_N} = c_{\sigma_1,...,\sigma_N} = \sum_{a_1}^{d'} \Psi_{\sigma_1,\sigma_2,...,\sigma_{N-1},a_{N-1}} R^{\sigma_N}_{a_{N-1}} = \sum_{a_1,...a_{N-1}} R^{\sigma_1}_{a_1} R^{\sigma_2}_{a_1,a_2} ... R^{\sigma_N}_{a_{N-1}} \tag{5.16}$$

From which we reach

$$\boxed{|\psi\rangle = \sum_{a_1,...,a_N} R^{\sigma_1} R^{\sigma_2} ... R^{\sigma_N} |\sigma_1, ...\sigma_N\rangle} \tag{5.17}$$

and, in turn, for the matrices R the following property applies

$$\boxed{\sum_{\sigma_l} R^{\sigma_l} R^{\sigma_l \dagger} = I} \tag{5.18}$$

If we wish, we can decompose the set of coefficients c as an arbitraty combination of left orthogonal and right orthogonal matrices, with the matrix containing the singular values in the middle. Let's say we re-write ψ with l left-orthogonal matrices and $N - l$ right orthogonal matrices, as in

$$|\psi\rangle = \sum_{\sigma_1,\ldots,\sigma_l,\ldots,\sigma_N} L^{\sigma_1}_{a_1} \ldots L^{\sigma_l}_{a_{l-2}a_{l-1}} S R^{\sigma_{l+1}}_{a_l a_{l+1}} \ldots R^{\sigma_{N-1}}_{a_{N-2}a_{N-1}} R^{\sigma_N}_{a_{N-1}}. \tag{5.19}$$

Diagramatically, this can be seen as in Fig.5.3.

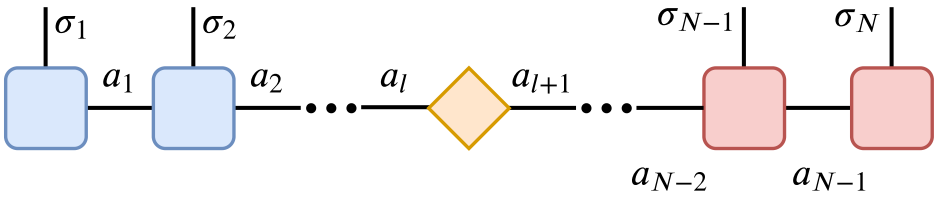

Figure 5.3: Diagramatic representation of a matrix product state composed of ℓ left-canonical matrices and $N - \ell$ right-canonical matrices. Here, the blue nodes are the left-canonical representation of the state, red nodes are the right-canonical parts, and the orange diamond contains the singular values.

Alternatively, by contracting back the matrix that holds the singular values with a neighboring matrix and performing a new SVD on the resulting matrix, one can "move" the diamond-shaped node left or right throughout the chain. The reason why one would want to do that is that operations regarding only left/right-orthogonal matrices are trivial, a consequence of properties 5.15 5.18 respectively. The position where the singular values are calculated is called the **orthogonality center**, and it sets the only non-trivial calculations to be made.

This is used by the DMRG algorithms to hugely speed up computations of local properties at every set of two sites, as contracting over two left normalized L-matrices or over

two right normalized R-matrices simply yields a Kronecker delta, as denoted in Fig.5.4

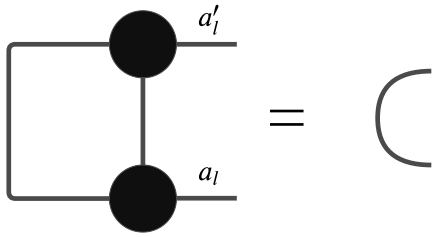

Figure 5.4: As setting up trivial contractions like these, one can hugely speed up calculations. Taken from Ref.[10].

The technicalities within the tensor structures are extremely important to correlate the physics to the numeric outline we've been stablishing. This is the foundation of the DMRG.

5.2.2 DMRG: iterative sweeping over the chain

The DMRG algorithm, however, is not done by a single SVD, but instead a sequential set of SVD's with subsequent truncations. This sequence of SVD's is called a *sweep* motion. The routine runs throughout the chain, performing SVD's and contractions to move the orthogonality center to the left, or to the right, and turning the neighboring matrices into left/right canonical. Up until this point, calculations can be exactly made. But as the chain size L increases, the dimension of the singular value matrix also increases with $L \times L$, and therefore it is not practical to look at the entirety of these matrices. To mitigate this problem, the routine reduces the dimension of these matrices by truncating over the smallest singular value(s). At this point, truncation error arises, as the payoff of having a feasible numerical algorithm. The number of singular values taken into account in one sweep is called the bond-dimension, as it dictates the dimension of the indices of the square matrix containing the singular values.

A step in this procedure can be seen as a diagram in Fig.5.5.

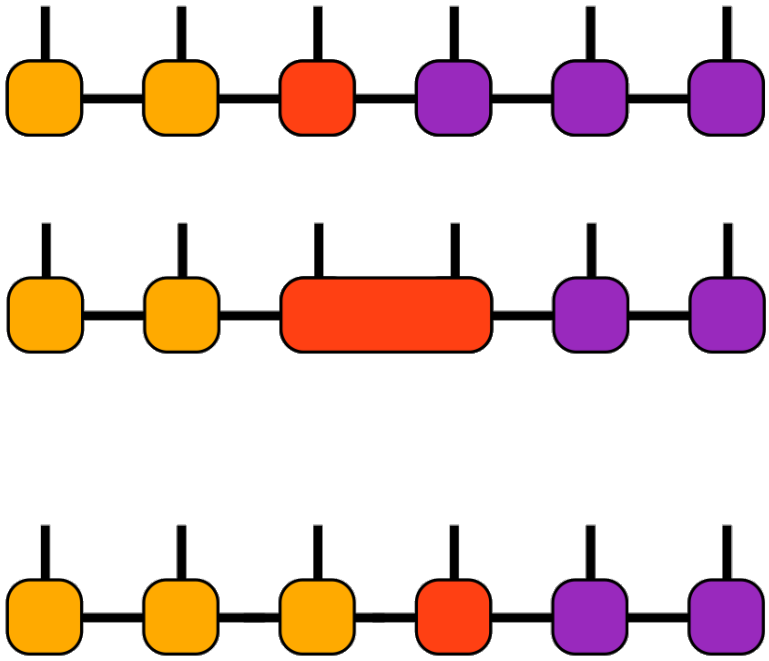

Figure 5.5: Sweep motion over the chain, from the left side to the right. The orange node contains the singular values being extracted from the SVD, and the yellow/purple nodes are left/right orthogonal, respectively. Taken from [26].

This effectively diminishes the dimension of the Hilbert Space in which the system exists. As discussed in 4.1, this is a keen guess, as by truncating over the smallest singular values, not much information of the system is lost. Additionally, as we discussed, the left/right orthogonal matrices are trivial to work with, and by focusing all the information in the singular value matrix S, applying an observable to the system is akin to applying it to a single site, or pair of sites. This makes the DMRG-based algorithms very cost effective, while incredibly useful for 1-dimensional systems.

5.3 Details of implementation

5.3.1 Vectorization and the Hilbert space

The above algorithm was designed for pure states and aims at finding the ground state of a given Hamiltonian. We now show how this very same idea can be generalized to compute the NESS of an open quantum spin chain. For that to work, though, the system needs to be vectorized, as the effective implementations that make use of DMRG routines excel when trying to solve these problems as operators acting on to vectors. As we reached Eq.3.4, we have a superoperator acting on a density matrix. And we therefore make use of the vectorization procedure stablished in Sec.2.2. By using Eq.2.15, we get, respectively for the Hamiltonian and for each term of the Dissipator:

- $-i[H,\rho] \longrightarrow -i(I \otimes H \left|\rho\right\rangle - H^T \otimes I \left|\rho\right\rangle)$
- $\sigma^+\rho\sigma^- \longrightarrow (\sigma^+ \otimes \sigma^+) \left|\rho\right\rangle$
- $\sigma^-\sigma^+\rho \longrightarrow (I \otimes \sigma^-\sigma^+) \left|\rho\right\rangle$
- $\rho\sigma^-\sigma^+ \longrightarrow (\sigma^+\sigma^- \otimes I) \left|\rho\right\rangle$
- $\sigma^-\rho\sigma^+ \longrightarrow (\sigma^- \otimes \sigma^-) \left|\rho\right\rangle$
- $\sigma^+\sigma^-\rho \longrightarrow (I \otimes \sigma^+\sigma^-) \left|\rho\right\rangle$
- $\rho\sigma^+\sigma^- \longrightarrow (\sigma^-\sigma^+ \otimes I) \left|\rho\right\rangle$

This leads us from the dynamics associated to 3.1 to

$$-i[H,\rho] = -i(I \otimes H - H^T \otimes I) \left|\rho\right\rangle \tag{5.20}$$

and the dissipative parcel from 3.2, by combining 2.34 and 2.35, to

$$\begin{aligned} D_j(\rho) = \Bigg[& \gamma f_j \Big[\sigma_j^+ \otimes \sigma_j^+ - \frac{1}{2} I \otimes \sigma_j^- \sigma_j^+ - \frac{1}{2} \sigma_j^+ \sigma_j^- \otimes I \Big] \\ & + \gamma (1 - f_j) \Big[\sigma_j^- \otimes \sigma_j^- - \frac{1}{2} I \otimes \sigma_j^+ \sigma_j^- - \frac{1}{2} \sigma_j^- \sigma_j^+ \otimes I \Big] \Bigg] \left|\rho\right\rangle . \end{aligned} \tag{5.21}$$

After this procedure, these can be easily implemented and worked on with the tensor network techniques. But there's more than one way to look at the same Hilbert Space, as we now discuss.

5.3.2 Rearranging the Hilbert space

As the non-locality that arrises from the presence of the environment poses a barrier to simulations, there's a need to vectorize the system of a one-dimensional chain in a smart way, so that this problem is mitigated. Let's look at how to do that effectively. Initially, let us revisit the Hamiltonian

$$\mathcal{H} = \sum_{i=1}^{N} (\sigma_i^x \sigma_{i+1}^x + \sigma_i^y \sigma_{i+1}^y + \Delta \sigma_i^z \sigma_{i+1}^z) + \sum_{i=1}^{N} h\sigma_i, \qquad \text{(3.3 revisited)}$$

and the dissipators D_j in Eq.5.21. Note that the Hamiltonian acts on each σ_j, σ_{j+1} whereas the dissipators act on σ_j, σ_j'. Now say we have a system composed of multiple spins, let us denote it as previously as

$$\rho = \sum_{i,j} \rho_{i,j} \left|i\right\rangle \left\langle j\right| . \tag{5.22}$$

As discussed previously, we can write a vectorized version of ρ as

$$\left|\rho\right\rangle = \sum_{i,j} \rho_{i,j} \left|j\right\rangle \otimes \left\langle i\right| , \tag{5.23}$$

There is not one single way to vectorize ρ, as we will show. If we write the indices i and j relating to the site operators $\sigma_1 ... \sigma_N$, we can re-write Eq.5.22 as

$$\rho = \sum_{i,j} \rho_{\sigma_1,...\sigma_N,\sigma_1',...,\sigma_N'} \left|\sigma_1, ..., \sigma_N\right\rangle \left\langle \sigma_1', ..., \sigma_N'\right| . \tag{5.24}$$

This can be perceived as in Fig.5.6.

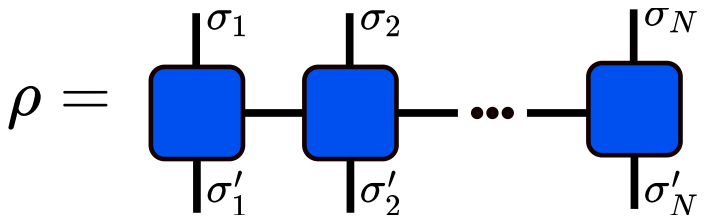

Figure 5.6: Each node has local information about each site. Upon contracting over the horizontal, indices (non-identified in the figure) one recovers ρ.

Here, the part regarding $\sigma_1, ..., \sigma_N, \sigma'_1, ..., \sigma'_N$ can be seen as

$$|\sigma_1, \sigma_2..., \sigma_N\rangle\langle\sigma'_1, \sigma'_2, ..., \sigma'_N| = |\sigma_1\rangle\langle\sigma'_1| \otimes |\sigma_2\rangle\langle\sigma'_2| \otimes ... \, |\sigma_N\rangle\langle\sigma'_N| \,, \tag{5.25}$$

which can be either mapped to

$$|\sigma'_1\rangle \otimes |\sigma_1\rangle \otimes |\sigma'_2\rangle \otimes |\sigma_2\rangle \otimes ... \, |\sigma'_N\rangle \otimes |\sigma_N\rangle \,, \tag{5.26}$$

or to

$$|\sigma'_1\rangle \otimes |\sigma'_2\rangle \otimes ... \, |\sigma'_N\rangle \otimes |\sigma_1\rangle \otimes |\sigma_2\rangle \otimes ... \, |\sigma_N\rangle \,. \tag{5.27}$$

In the physical sense this makes no difference, the problem is the same, just mapped differently. Although, if we map the system as in Eq.5.27, the vectorized version of ρ,the interactions of the Hamiltonian are diagramatically depicted in Fig.5.7, the orange lines representing where each part of the Hamiltonian act on.

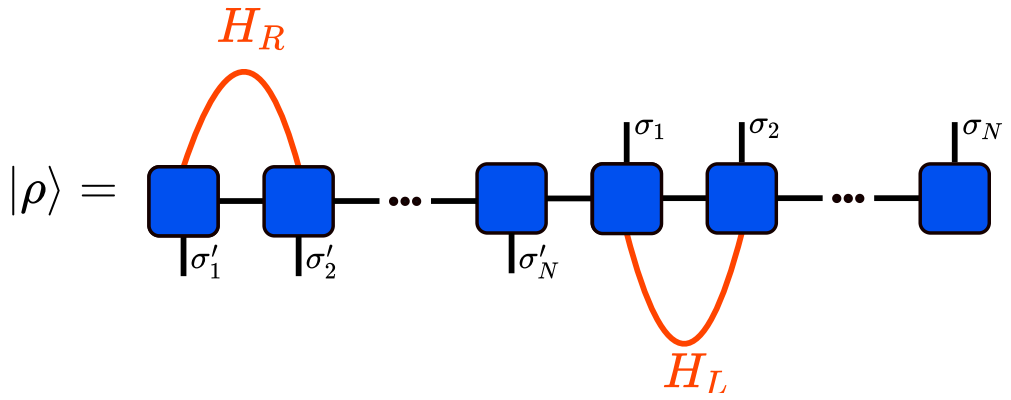

Figure 5.7: Schematics of the local Hamiltonian interaction on a density matrix ρ if the system is structured as in Eq.5.27. In this picture, it is akin to first neighbor interactions.

Where H_R and H_L are the portion of the Hamiltonian acting on the right and left part of the vectorized version of the system. This means that, in this mapping, the Hamiltonian acts locally in each pair of MPS. The dissipators, however, as noted in Eq.5.21, act on each pair $\sigma_j\sigma'_j$, which makes it highly non-local as σ_j and σ'_j are separated by $N-1$ sites, making it a $N-1$ neighbor interaction. This can diagramatically be seen in Fig.5.8.

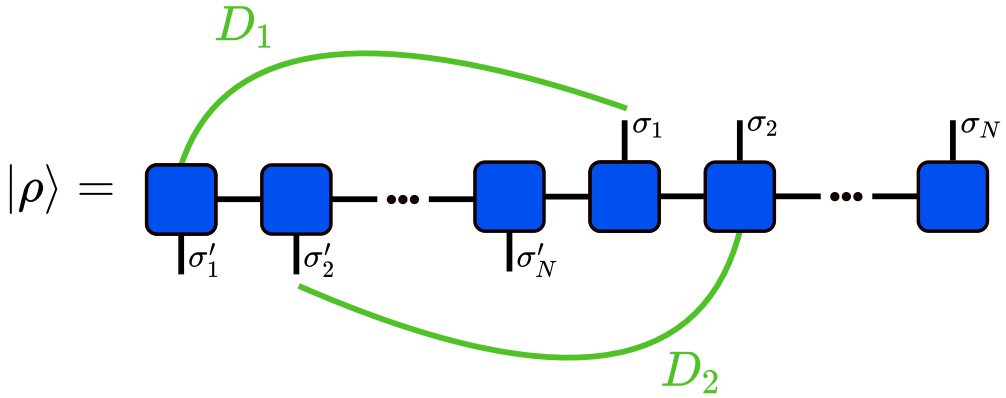

Figure 5.8: The structure of ρ, based around Eq.5.27 make it so that the dissipators act highly non-locally.

On the other hand, if we structure ρ as depicted in Eq.5.26, the Hamiltonian would, instead, act akin as a second neighbor interaction, as shown in Fig.5.9.

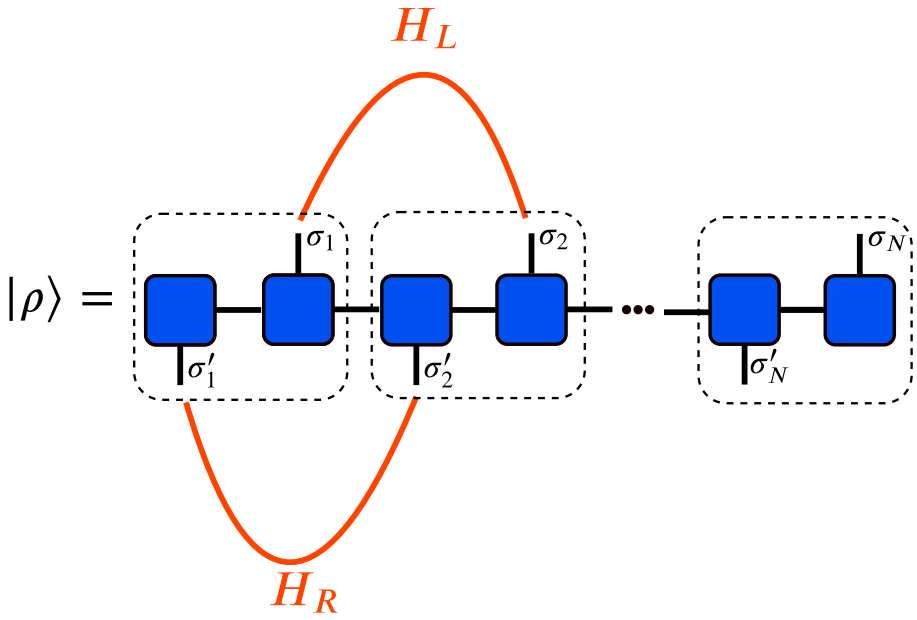

Figure 5.9: Schematics of the local Hamiltonian interaction on a density matrix ρ if the system is structured as in Eq.5.26. The dashed box shows how can one easily recover the initial density matrix tensor, by contracting the two sites inside the box.

This means that the Hamiltonian acts *slightly* non-locally, being mapped as a second neighbor interaction. The dissipators, however, act on each pair $\sigma_1 \longleftrightarrow \sigma'_1$, as depicted in Fig.5.10.

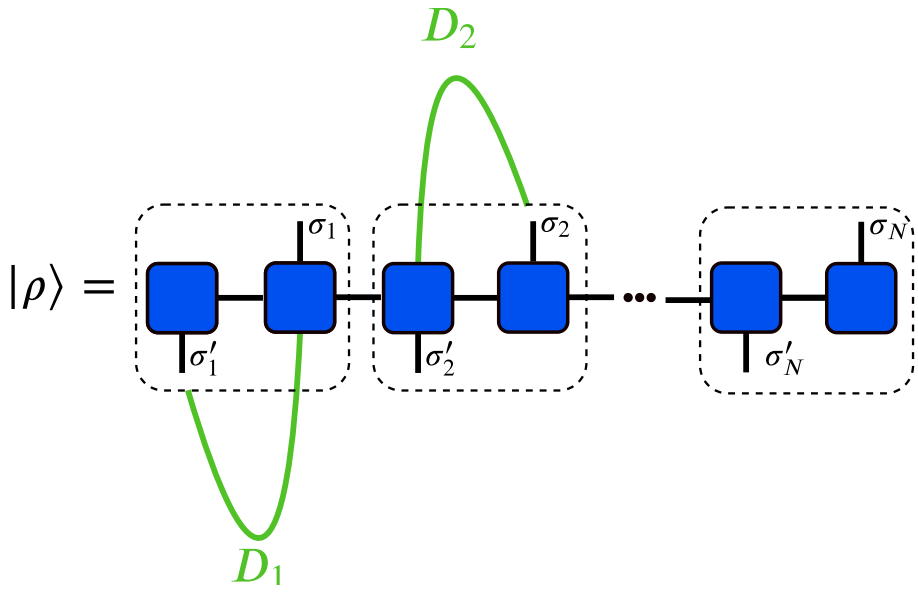

Figure 5.10: Schematics of the Dissipators acting on a density matrix ρ if the system is structured as in Eq.5.26. The dashed box shows how can one easily recover the initial density matrix tensor, by contracting the two sites inside the box.

The dissipators would act on each pair of sites, immediately next to each other, making it akin to a first neighbor interaction.

If we were to derive the MPS of ρ following 5.27, we would be forced to use a $2L$ sized chain when simulating, as there's no way to simplify it. We will therefore call the structure depicted in Fig.5.7 and Fig.5.8 $\mathbf{2L}$ **formalism**. As for Eq.5.26, which spans the depiction in Fig.5.9 and Fig.5.10, we will call it the $\boldsymbol{L}$ **formalism**, as we are able to contract each neighboring sites into a single tensor with two indices, σ_j, σ'_j, therefore recovering a L sized-chain.

As we will see now, the L formalism is usually better than the $2L$ formalism due to the more localized nature of the dissipators.

L x *2L* - Choosing the right Hilbert space structure

There are now two distinct ways to frame how the MPS ansatz will treat the system, which we referred to as the $2L$ and L formalisms following Sec.5.3.2. A comparison of both formalisms is shown in Fig.**??**, where we plot the NESS energy guess as a function of the number of sweeps for different chain sizes.

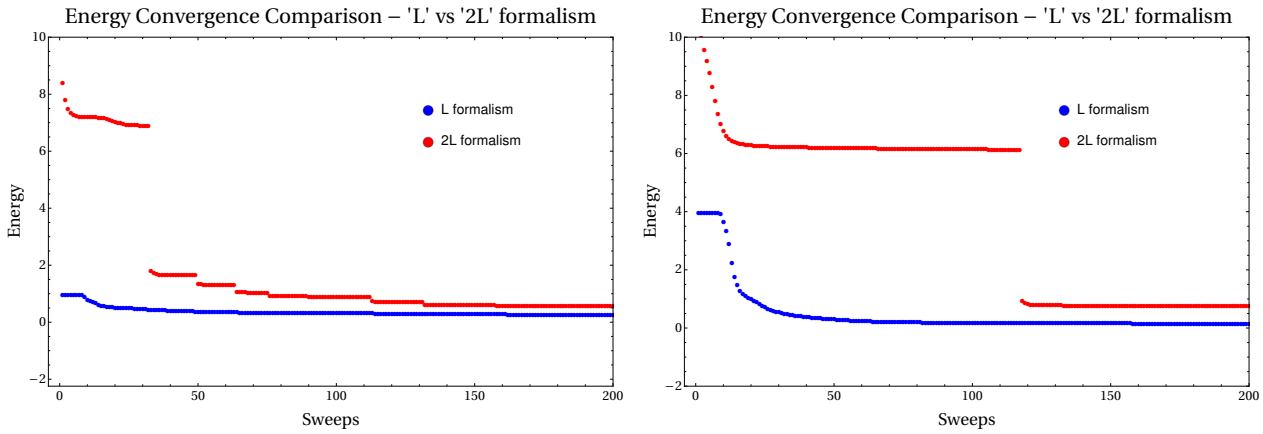

(a) $L = 50$ (b) $L = 200$

Figure 5.11: Ground state convergence L x 2L formalism comparison, for different spin lenghts L. The parameters used in this set of simulations were $\gamma = 4, f_1 = 0.49, f_L = 0.51, h = 0, \Delta = 0.1$.

For small sizes ($L \leqslant 50$) both methods seem to converge, although the *2L* formalism is still slightly worse in comparison. The pay-off is that the *L* formalism takes comparatively more time/sweep than the *2L*, but as the chain size increases, it becomes harder to compute the dissipators role in the dynamics if we use the *2L* structure, and the NESS energy guess is significantly worse compared to the *L* counterpart. The same is not true for the *L* structure, where the NESS energy guess is more accurate in comparison, and presents a smooth, controlled and constantly improving guess after each sweep. For open system simulations, therefore, Eq.5.26 poses as a better guess, especially in the treatment of bigger chains. In the following results, we have choosen to use the *L* formalism.

Chapter 6

Numerical results

6.1 Initial state guess and the the warm-up routine

The ITensor library initializes a random configuration of spins upon creating the MPS object. This makes it hard to benchmark one simulation against another, as they don't start in the same exact place. Additionally, not every MPS vector can represent a valid physical state. For this reason every initial state is set up to be the identity vector, as it satisfies the normalization condition, and is Hermitian.

After implementing the operators as MPOs and the Heinserberg chain as an MPS, and then choosing a feasible physical state to start the simulation with, we then implemented a warm up routine, in which the bond dimension in the simulation is the lowest one possible, which is 1. Here, DMRG sweeps are made up to the point where the energy before and after a sweep have converged to the same value under a 1% error which means the bond-dimension 1 have saturated, and therefore the simulation cannot be significantly improved further. This way, the number of sweeps in the warm-up routine depends from simulation to simulation. This particular step yields for better simulation times, as low bond dimensional sweeps are very easy to perform, since the computer has just one dimensional matrices to compute. This is also perceived as a better initial guess. We have ran a set couple of routines to test how this affects the simulation. This is depicted in Fig.6.1.

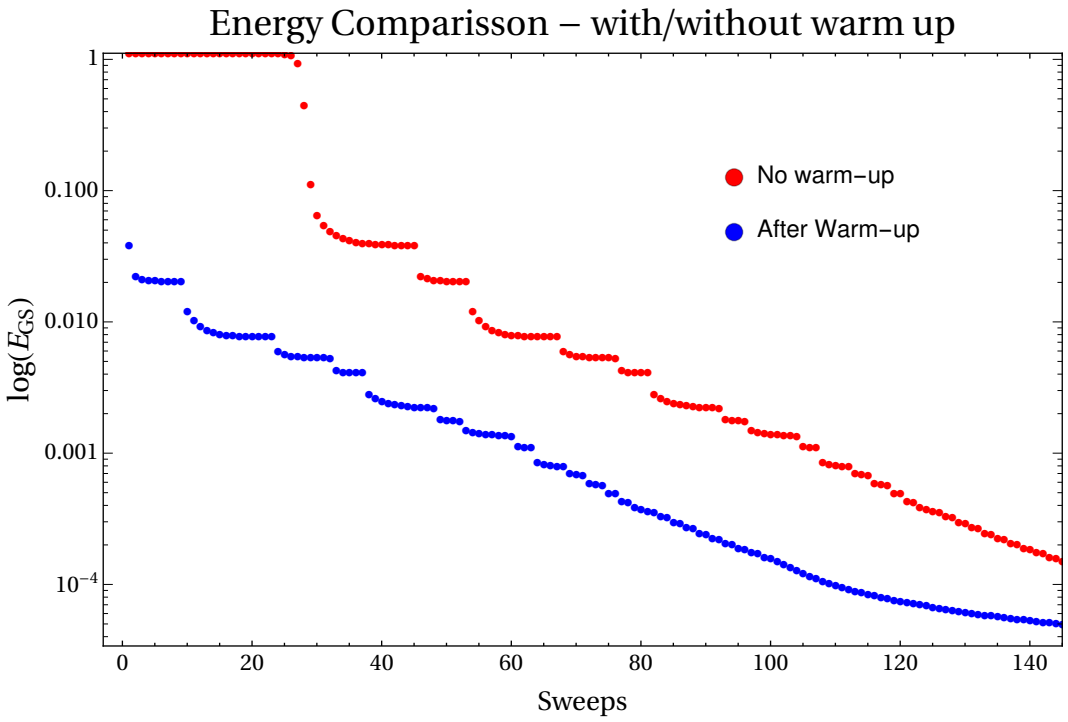

Figure 6.1: Comparison of how the warm up routine sharpens the guess of the ground state energy. Values used: $L = 10, \gamma = 1, f_1 = 1, f_L = 0, h = 0, \Delta = 1$

By using the warm-up routine before letting the DMRG attain for bigger dimensions, more singular values, one can have, in less computation time, better results, as the system is slowly steered into a better guess of the ground state. This takes very little time, as shown in Fig.6.2.

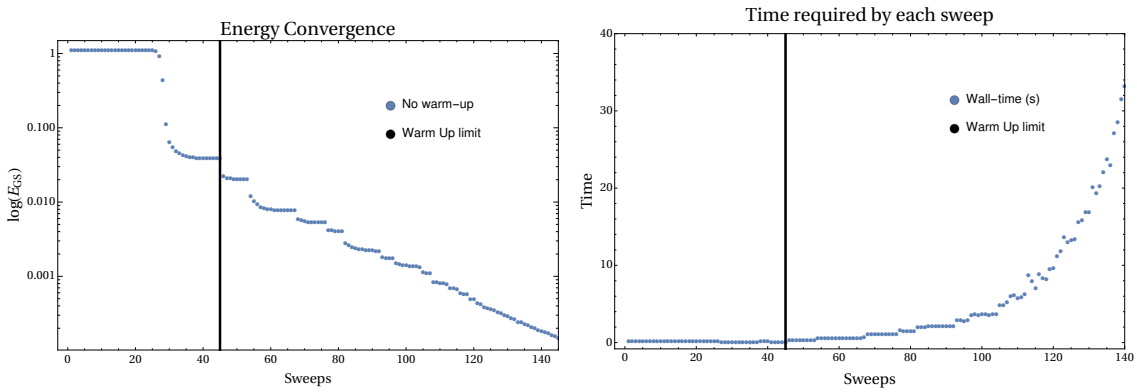

(a) Ground State Energy after each sweep

(b) Time demanded by each sweep

Figure 6.2: Plots of both ground state energy and time taken by sweep per sweep. Values used: $L = 10, \gamma = 1, f_1 = 1, f_L = 0, h = 0, \Delta = 1$

As the time it takes to sweep over the chain is minimal when the bond dimension is one, it's optimal to use it to a sharper initial guess, which can then be refined by the algorithm.

6.2 Code implementation

We present snippets of the final version of the code developed by us, among with brief explanations.

Initially, the code stablishes values for the size L of the chain, the coupling γ, the temperatures f_1 and f_L of the baths in site one and L, the magnetic field acting over the chain h and the anisotropy Δ, as well as the vectors used to store information of the simulation. The input values $L, \gamma, f_1, f_L, h, \Delta$ are all decided by the user. Two more technical values, the dimension of the bond used by the SVD 5.1 and the sweeps made with such bond value by the DMRG routine 5.2, are determined by the algorithm to assure convergence. If no constraint is set the code will run indefinetly, increasing the bond dimension and sweeping indefinetely, trying to reach a more accurate configurations of the NESS.

We have created the TwoSpinHalf() environment to structure the system indices in the *L* formalism. Even though this formalism is, as discussed in Sec.5.3.2 better, we have implemented the same version with the *2L* counterpart structure. In that case, the algorithm uses already implemented SpinHalf() function to create the sites containers. After creating the indices, the MPS representation of the chain, ρ_L, is created by a built-in function of the ITensor, with appropriate fitting indexes. This is represented in the code that follows.

```
SiteSet sites_L = TwoSpinHalf(L);
auto rho_L = MPS(sites_L);
```

The Liouvillian $\mathcal{L}$ is then constructed following the desired input, as well as $\mathcal{L}^\dagger$, and the operator $\mathcal{L}^\dagger\mathcal{L}$ is stored in $M2$.

```
//constructing M by  L(dag)*L
AutoMPO LiouvAMPO_L = LiouvConstruct_L(gamma, f1, fL, h, Delta, sites_L);
AutoMPO LiouvDAMPO_L = LiouvDConstruct_L(gamma, f1, fL, h, Delta, sites_L);

MPO Liouv_L = MPO(LiouvAMPO_L);
MPO LiouvD_L = MPO(LiouvDAMPO_L);
MPO M2;
nmultMPO(Liouv_L, LiouvD_L, M2, {"Maxm", 50000,"Cutoff",1E-8}); // constructs M = Ld*L
```

The functions LiouvConstruct_L, LiouvDConstruct_L were built with code-like versions of the instances stablished back in Sec.3.

A first step of simulations is run in the *warm up* routine Finally, a loop is set to run through DMRG calculations, sharpening the guess of the NESS, as demonstrated below.

```
for (int i = 0; tag; i += sweepNumber)
{
    auto energyIni = energy2;
    energy2 = dmrg(rho_L,M2,sweeps,{"Quiet",true});
    auto energyFin = energy2;


    if (energyIni-energyFin < sweepBDChangeThresholdValue)
    {
        std::cout << "\n\nEndedWarmUpAfter " << i << " sweeps \n\n ";
        tag = false;
    }
}
```

6.3 The bond-dimension and how to increase it

After each sweep, if the difference between the energy calculated after the sweep and the energy calculated before it falls under 1% of the initial energy, the bond dimension is increased by one. This means that the smaller bond-dimension has saturated its capabilities of describing the system accurately. This can be seen as jumps in Figs.6.1 and 6.7.

It is important to note that inadvertently raising the bond dimension may deem the simulation unviable, or make it diverge. For instance, observables that should be real may have complex parts.

A simulation where this happens can be found in Figs.6.3 and .6.4.

In this set of simulations the parameters used were $\gamma = 1, f_1 = 1, f_L = 0, h = 0, \Delta = 1$, and therefore, analytical values are available.

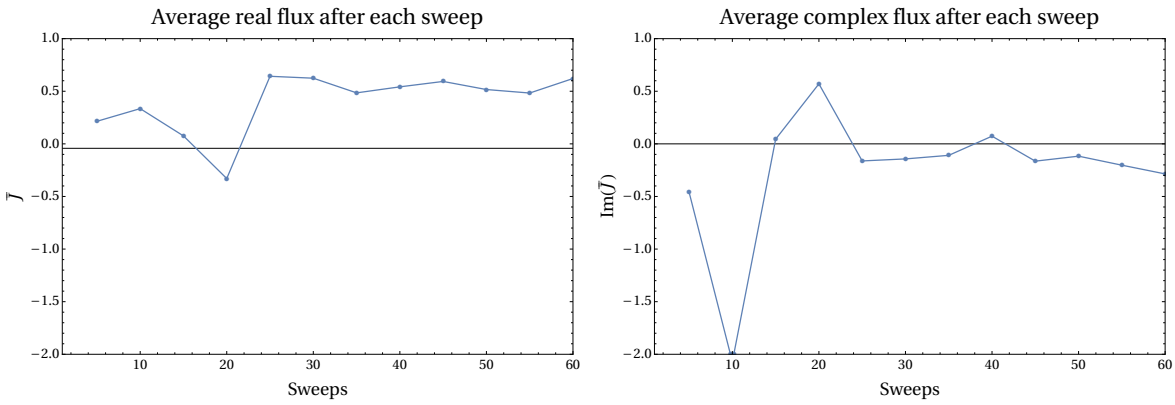

(a) (b)

Figure 6.3: Example the spin flux output of a simulation in which the bond dimension increases uncontrolably. The spin flux, which is strictly real, in this simulation has a significant complex parcel, and it does not show signs of convergence. Instead, at sweep $= 50$ it appears to diverge. In 6.3a the gray line represents the analytical value of the flux, in this case, of (-0.0422982). In 6.3b The grey line marks the zero, which is expected for the complex part of it. Values used: $L = 30, \gamma = 1, f_1 = 1, f_L = 0, h = 0, \Delta = 1$.

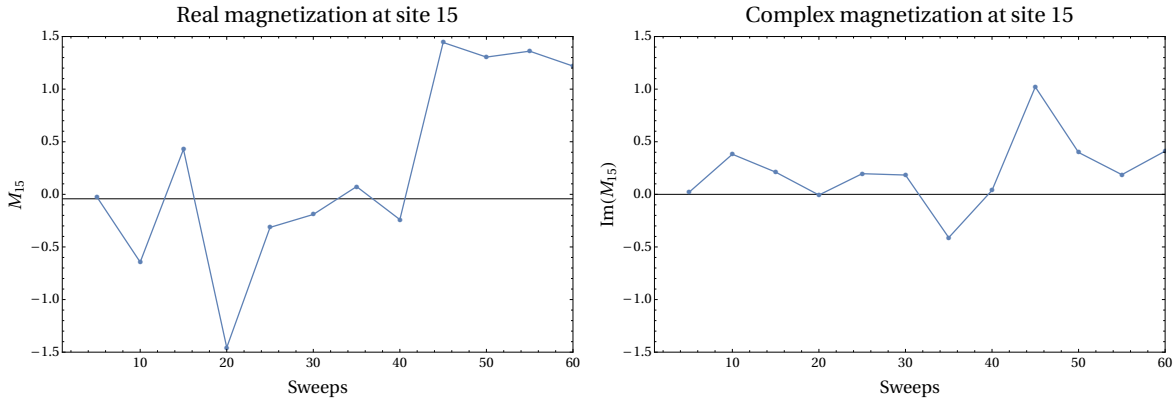

(a) (b)

Figure 6.4: Example of a simulation in which the bond dimension increases uncontrolably. As before, the magnetization which is also real, also has a significant complex parcel.In both plots the magnetization was calculated at site $s = 15$. In 6.4a the grey line represents the analytical value of (-0.0496188). In 6.4b the expected value is zero, as the magnetization should be real. Values used: $L = 30, \gamma = 1, f_1 = 1, f_L = 0, h = 0, \Delta = 1$.

This particular simulation has clearly run out of control. The cause for this is the unwise increments in the bond dimension. In this case, the initial bond dimension was 10 and after each sweep the bond-dimension was increased by 10. Upon correcting this, much more satisfying results arise. They are compilled in Figs.6.5 6.6.

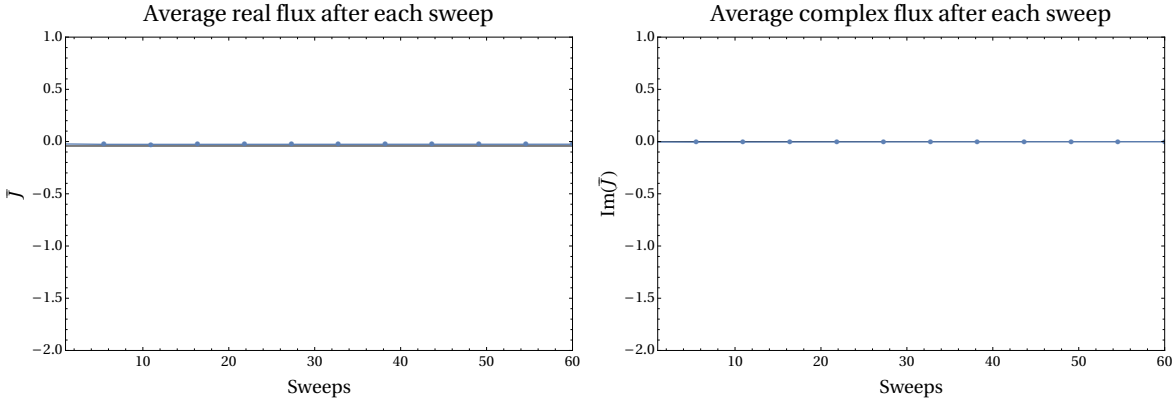

(a) (b)

Figure 6.5: Example of a simulation in which the bond dimension increases in a controlled manner, attaining for good spin flux results. In this set of simulations the spin flux converges nicely to the expected value (6.5a) and the complex part stay near zero (6.5b), as one would expect. Values used: $L = 30, \gamma = 1, f_1 = 1, f_L = 0, h = 0, \Delta = 1$.

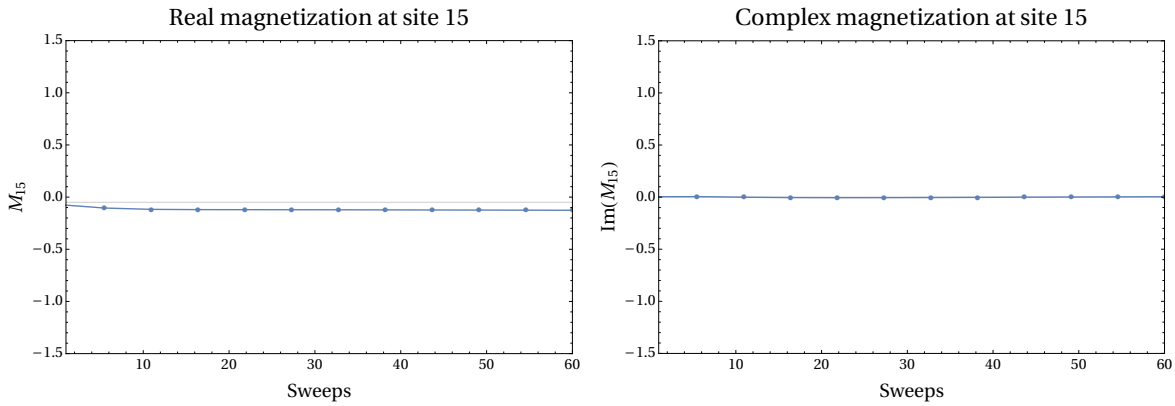

(a) (b)

Figure 6.6: Example of a simulation in which the bond dimension increases in a controlled manner, attaining for good magnetization results. In this set of simulations, the magnetization stays near the expected value and the complex part stay near zero, as expected. Values used: $L = 30, \gamma = 1, f_1 = 1, f_L = 0, h = 0, \Delta = 1$.

Note that in both of these cases, only 60 sweeps were made, and thus it is not expected a 30 sites simulation to fully converge. But the difference is clear. One should be careful of the increments of the bond-dimension throughout the simulation. The routine in which the bond dimension increases by increments of 10 also, as one would expected, takes way longer to compute each sweep.

6.4 Convergence to the non-equilibrium steady state

Naturally, the first step after succefully implementing the algorithm is to see if it is working properly, and since that we pursue the eigenstate with eigenvalue zero as discussed, we can actually pinpoint the convergence by calculating the energy after each sweep. For instance, and for various spin-chains lengths, one can see that the NESS ground energy converges nicely for sizes up to $L = 50$.

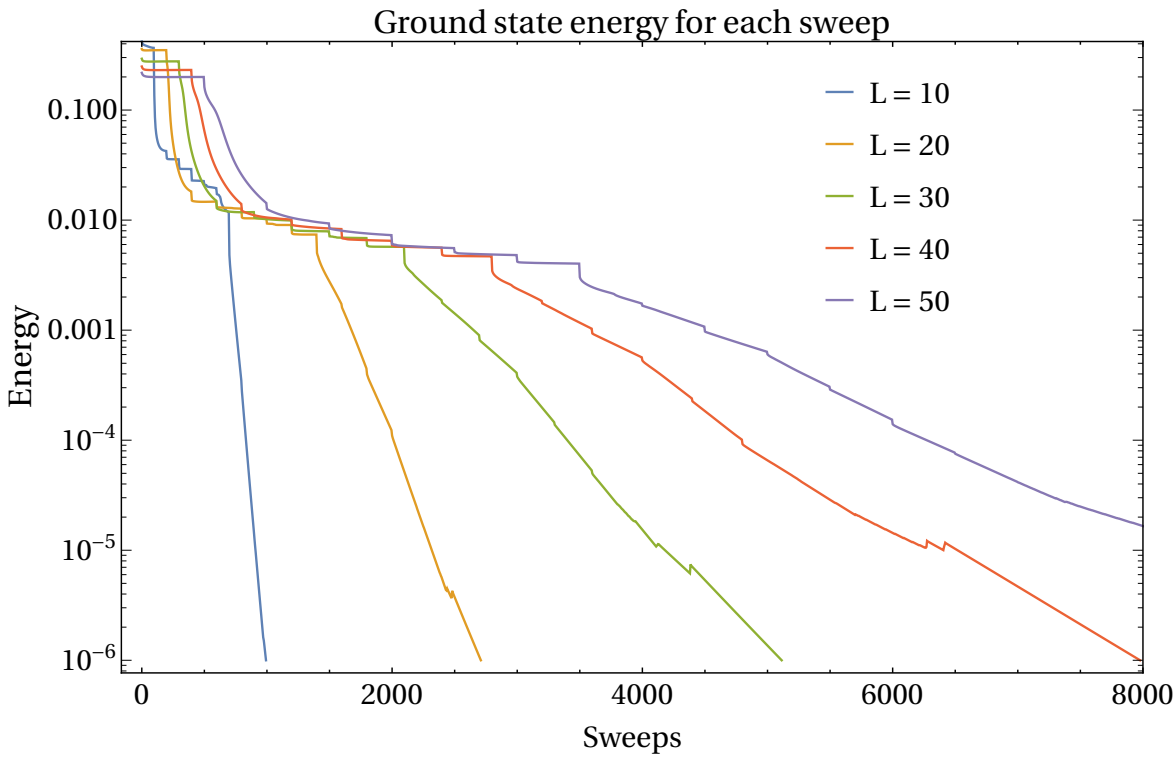

Figure 6.7: As the chain size increases, the algorithm naturally takes longer to converge. The Y axis presents a log plot of the energy value. This set of simulations used $\Delta = 0.5, \gamma = 1, f_1 = 1, f_L = 0$

6.5 Analytical benchmarking, novel results

As discussed in Sec.3.3, when the anisotropy term is trivially 1, the analytical results can be directly computed for specific conditions of the baths ($f_1 = 1, f_L = 0$), as in Refs.[22] and [23]. We have plotted these values as well as the simulation spin flux (y) after each sweep (x) in Fig.6.8.

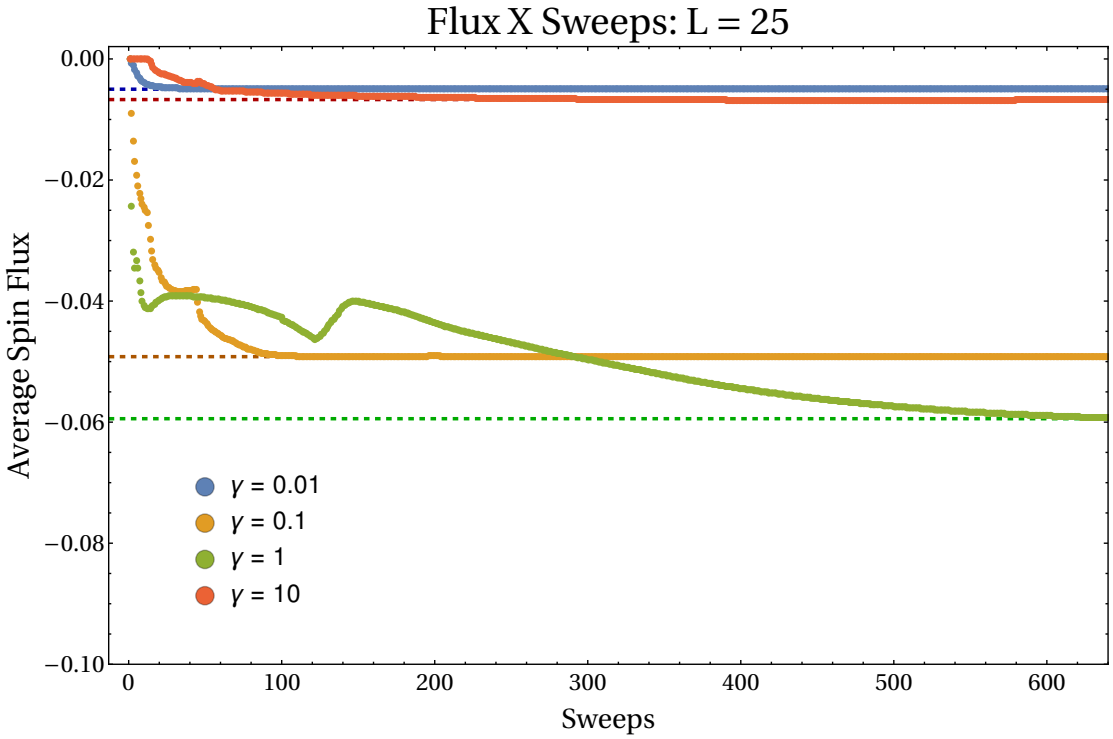

Figure 6.8: The analytical values are seen in dashed lines. The Y axis presents the average spin flux throughout the chain. This set of simulations was made using $L = 25, \Delta = 0.1, f_1 = 1, f_L = 0$

For smaller and larger values of γ the simulation needs less than 200 sweeps to fully converge. For intermediate values, however, it takes longer. In both cases a steady approximation to the analytical values is noted.

Additionally, by looking at the spin flux for different chain lenghts, we are able to see the transition between the ballistic transports for $L \sim 10$ to diffusive for $L = 15$ onwards. This is depicted in Fig.6.9.

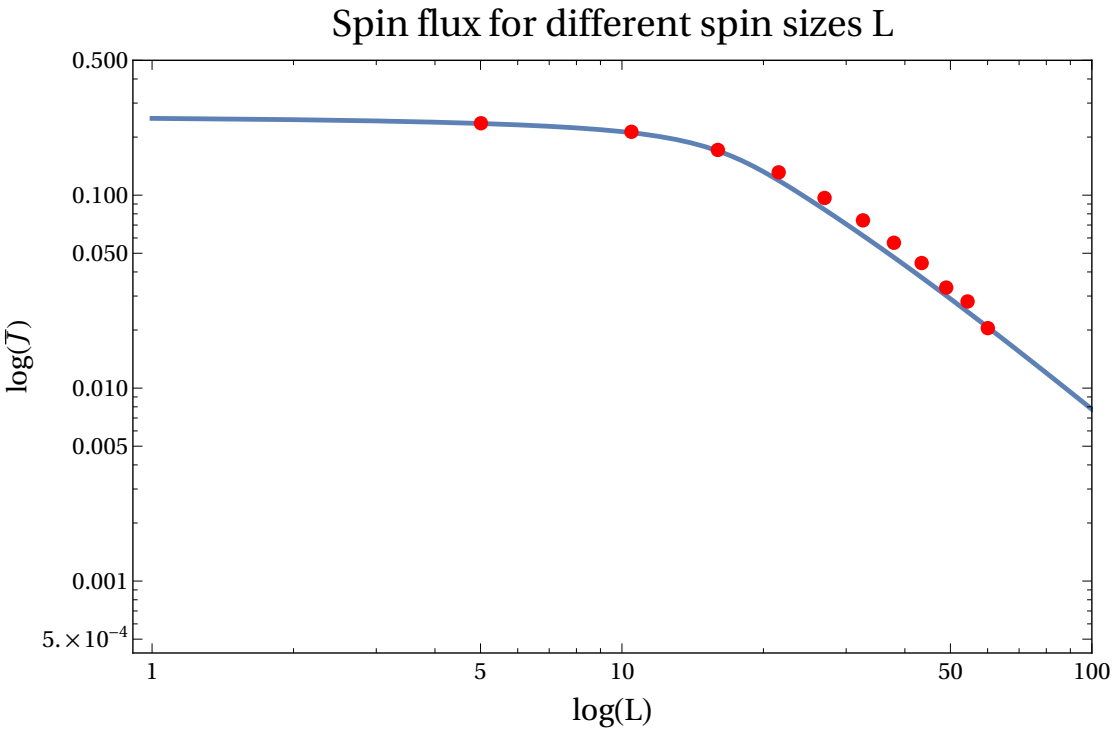

Figure 6.9: Varying flux for different lenghts of spin chain, up to L = 100. The blue line follows the analytical results derived from Ref.[17]. This set of simulations was made with $\gamma = 0.5, \Delta = 1, f_1 = 1, f_L = 0$

The dependence of the spin flux with different γ, is also an interesting question. This was approached in simulations depicted in 6.10.

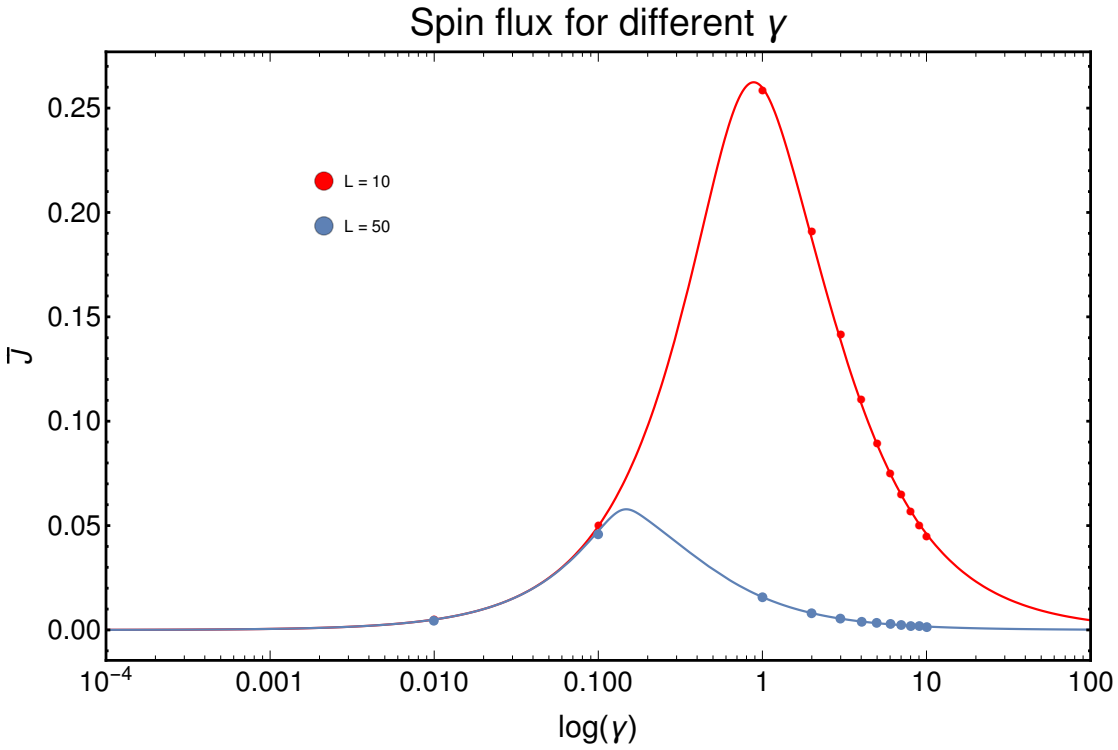

Figure 6.10: Varying flux for different values of γ. The solid lines follow the analytical results derived from [17]. This set of simulations was made with $\Delta = 1, f_1 = 1, f_L = 0, h = 0$

As there were also analytical results, it is a nice fit between the simulations and whats expected.

These results are quite interesting for they provide a working, feasible implementation of the DMRG technique in the framework of open systems.

Chapter 7

Final remarks and next steps

In this work, we have developed a working and efficient algorithm, that requires no broad computational power, based upon state-of-the-art results regarding numerical simulations of one-dimensional open quantum systems. We have analysed the role that the vectorization procedure plays in how efficiently such simulations develop, as well as how the numerical parameters control the accuracy of DMRG calculations, namely the sweeps performed by the DMRG algorithm and the bond dimension used in the approximations.

We have benchmarked the code against available numerical results, and such benchmarking proved the algorithm to be working as expected. We have implemented procedures to diminish error by taking into account how to evolve the simulation, choosing appropriate bond dimension values and an appropiate initial physical state to control the evolution. Regarding the physics, we have been able to study systems of different sizes, up to $L = 60$ (althought the algorithm is also fully functional for bigger sizes, up to 200), as well as different coupling factors γ. We have studied the spin flux in such cases, and found it to be in agreement with the available literature. In this sense, our contribution by this work makes it possible to study more complex combinations of parameters, which is not achievable analytically. This prospect is quite exciting for us in both physical and computational sense. Numerous scenarios may now be extended and studied effectively, taking into account chain sizes, magnetic fields, different bath's temperatures, coupling factors and anisotropies configurations. We intend to probe these problems in the near future.

Additionally, although not the focus of this work, we have also successfully implemented a functional routine for the Trotter gates time evolution deriving it from the available ITensor code.

To our knowledge, this is the first code broadly applicable and viable to large chain-sizes developed by a group from Brazil in the study of open quantum systems. The code is freely available upon request.

The XXZ system is extremely rich, and interesting new phenomena may be lurking in the frontier of computational simulations. We hope that this work may be used to explore this frontier further.

Bibliography

[1] H. P. Breuer and F. Petruccione, *The theory of open quantum systems*.

[2] E. Schrdinger, "Discussion of probability relations between separated systems," *Mathematical Proceedings of the Cambridge Philosophical Society*, vol. 31, no. 4, p. 555563, 1935.

[3] T. c. v. Prosen, "Open xxz spin chain: Nonequilibrium steady state and a strict bound on ballistic transport," *Phys. Rev. Lett.*, vol. 106, p. 217206, May 2011.

[4] J. Eisert, M. Friesdorf, and C. Gogolin, "Quantum many-body systems out of equilibrium," *Nature Physics*, vol. 11, p. 124, feb 2015.

[5] J. I. Cirac and P. Zoller, "Quantum computations with cold trapped ions," *Phys. Rev. Lett.*, vol. 74, pp. 4091–4094, May 1995.

[6] V. Balachandran, G. Benenti, E. Pereira, G. Casati, and D. Poletti, "Perfect Diode in Quantum Spin Chains," *Physical Review Letters*, vol. 120, no. 20, pp. 4–9, 2018.

[7] P. Gombás, "Zur theorie der metalle," *Hungarica Acta Physica*, vol. 1, no. 2, pp. 1–33, 1947.

[8] R. J. Baxter, *Exactly Solved Models in Statistical Mechanics*. 1984.

[9] D. Gobert, C. Kollath, U. Schollwöck, and G. Schütz, "Real-time dynamics in spin-$\frac{1}{2}$ chains with adaptive time-dependent density matrix renormalization group," *Phys. Rev. E*, vol. 71, p. 036102, Mar 2005.

[10] U. Schollwöck, "The density-matrix renormalization group in the age of matrix product states," *Annals of Physics*, vol. 326, no. 1, pp. 96–192, 2011.

[11] J. J. Mendoza-Arenas, "Spin and energy transport in boundary-driven low-dimensional open quantum systems," 2014.

[12] J. Cui, J. I. Cirac, and M. C. Bañuls, "Variational Matrix Product Operators for the Steady State of Dissipative Quantum Systems," *Physical Review Letters*, vol. 114, no. 22, pp. 1–5, 2015.

[13] S. R. White, "Density matrix formulation for quantum renormalization groups," *Physical Review Letters*, vol. 69, no. 19, pp. 2863–2866, 1992.

[14] S. R. White, "Density matrix renormalization group algorithms with a single center site," *Physical Review B - Condensed Matter and Materials Physics*, vol. 72, no. 18, pp. 1–4, 2005.

[15] M. Srednicki, "Entropy and area," *Phys. Rev. Lett.*, vol. 71, pp. 666–669, Aug 1993.

[16] *ITensor Library (version 2.0.11) http://itensor.org*.

[17] G. T. Landi, E. Novais, M. J. De Oliveira, and D. Karevski, "Flux rectification in the quantum XXZ chain," *Physical Review E - Statistical, Nonlinear, and Soft Matter Physics*, vol. 90, no. 4, pp. 1–11, 2014.

[18] B. Sutherland, *Beautiful Models*. WORLD SCIENTIFIC, 2004.

[19] D. Karevski and T. Platini, "Quantum nonequilibrium steady states induced by repeated interactions," *Phys. Rev. Lett.*, vol. 102, p. 207207, May 2009.

[20] T. Prosen and M. Žnidarič, "Matrix product simulations of non-equilibrium steady states of quantum spin chains," *Journal of Statistical Mechanics: Theory and Experiment*, vol. 2009, p. P02035, feb 2009.

[21] M. Žnidarič, "Spin transport in a one-dimensional anisotropic Heisenberg model," *Physical Review Letters*, vol. 106, no. 22, pp. 3–6, 2011.

[22] G. T. Landi and D. Karevski, "Open Heisenberg chain under boundary fields: A magnonic logic gate," *Physical Review B - Condensed Matter and Materials Physics*, vol. 91, no. 17, pp. 1–6, 2015.

[23] D. Karevski, V. Popkov, and G. M. Schütz, "Exact matrix product solution for the boundary-driven lindblad xxz chain," *Phys. Rev. Lett.*, vol. 110, p. 047201, Jan 2013.

[24] Y. Ge and J. Eisert, "Area laws and efficient descriptions of quantum many-body states," *New Journal of Physics*, vol. 18, p. 083026, aug 2016.

[25] E. M. Stoudenmire and S. R. White, "Minimally entangled typical thermal state algorithms," *New Journal of Physics*, vol. 12, p. 055026, may 2010.

[26] R. M. Noack, "Diagonalization- and numerical renormalization-group-based methods for interacting quantum systems," *AIP Conference Proceedings*, 2005.